1 *The author team submitted the following manuscript revision to Earth Surface Processes and Landforms*
2 *(ESPL) on Sept 29, 2020. This version comprises the first revision to this manuscript originally submitted*
3 *for publication in ESPL in March of 2020.*
4
5   - - - - - - - - -
6
7 **Rapid Tidal Marsh Development in Anthropogenic Backwaters**
8
9 **Key Points**:

10   1. Shoreline development along a major urban estuary served as the primary trigger for freshwater
11   tidal wetland development.
12   2. Marshes have developed and expanded rapidly in shallow settings after structures reduced
13   hydrodynamic energy and increased sediment trapping efficiency.
14   3. Stratigraphic evidence and historical maps and aerial photos show that more than half of the
15   tidal marsh area in the Hudson River developed in response to shoreline modification.

16 **Authors**

17 Brian Yellen[1], Jonathan Woodruff[1], Caroline Ladlow[1], David K. Ralston[2], Sarah Fernald[3], Waverly Lau[1]

18 **Affiliations**

19 [1]University of Massachusetts, Amherst, MA, USA

20 [2]Woods Hole Oceanographic Institution, Woods Hole, MA, USA

21 [3]New York State Department of Environmental Conservation, Hudson River National Estuarine Research
22 Reserve, Staatsburg, NY, USA

23 *For Earth Surface Processes and Landforms, first revision, Sept 2020.*

24 **Abstract**

25 Tidal marsh restoration and creation is growing in popularity due to the many and diverse set of services
26 these important ecosystems provide. However, it is unclear what conditions within constructed settings
27 will lead to the successful establishment of tidal marsh. Here we provide documentation for widespread
28 and rapid development of tidal freshwater wetlands for a major urban estuary as an unintended result
29 of early industrial development. Anthropogenic backwater areas established behind railroad berms,
30 jetties, and dredge spoil islands resulted in the rapid accumulation of clastic material and the
31 subsequent initiation of emergent marshes. In one case, historical aerial photos document this
32 transition occurring in less than 18 years, offering a timeframe for marsh development. Accretion rates
33 for anthropogenic tidal marshes and mudflats average 0.8-1.1 cm yr^{-1} and 0.6-0.7 cm yr^{-1} respectively,
34 equivalent to 2-3 times the rate of relative sea level rise as well as the observed accretion rate at a
35 6000+ year old reference marsh in the study area. Paired historical and geospatial analysis revealed that
36 more than half of all the tidal wetlands on the Hudson River were likely triggered by anthropogenic
37 development since the onset of the industrial era, including two thirds of the emergent cattail marsh.
38 These inadvertently constructed tidal wetlands currently trap roughly 6% of the Hudson River's
39 sediment load. Results indicate that when sediment is readily available freshwater tidal wetlands can
40 develop relatively rapidly in sheltered settings. The study sites serve as useful examples to help guide
41 future tidal marsh creation and restoration efforts.

42

1. Introduction

Tidal marshes provide many well-documented ecosystem services including habitat or forage for important fisheries (Boesch and Turner, 1984; Kneib, 1997; Minello et al., 2012), filtering and detoxifying terrestrial runoff (Brin et al., 2010; Nelson and Zavaleta, 2012), and buffering coasts from wave energy and storms (Cochard et al., 2008; Gedan et al., 2011; Knutson et al., 1982). At the same time, tidal marshes face several threats, most notably from accelerating sea level rise (Crosby et al., 2016; Törnqvist et al., 2020), reductions in sediment supply (FitzGerald and Hughes, 2019), impediments to landward migration (Schuerch et al., 2018; Spencer et al., 2016; Thorne et al., 2018), and land reclamation (Lewis et al., 2019; Gu et al., 2018). Marsh peats found well below present day sea level in off-shore settings provide examples of marshes that did not keep pace with prehistoric sea level rise (Emery et al., 1965; Wolters et al., 2010). Marshes that have survived have done so by migrating inland to higher elevation substrate or by accreting organic material and mineral sediment in order to maintain surface elevation close to mean high tide. Disruptions in sediment supply to the coast due to trapping behind dams (Blum and Roberts, 2009) compound threats posed by accelerated sea level rise. Reduced sediment supplies due to improved agricultural practices (Kirwan et al., 2011) and hardening of shorelines (Peteet et al., 2018) have also been linked to tidal marsh deterioration.

Humans have long modified the coastline for agricultural purposes, with the dike-polder landscape of Northern Europe presenting perhaps the most prominent example (Meier, 2004); however examples exist along many low-lying coastlines, including those of Bangladesh (Ali, 2002), China (Yan et al., 2019), Vietnam (Biggs, 2012), and elsewhere. The well-documented means of polder construction in Northern Europe consisted of brushwood groins built across tidal flats in order to reduce wave activity and currents, thereby enhancing sedimentation and initiating marsh growth (Meier, 2004). Due to the abundant sediment supply in areas of the North Sea, this brushwood groin technique was particularly effective, initially increasing tidal flat elevations by 5-15 mm/yr (Nolte et al., 2013), and by as much as 30 cm in less than a given year (Hofstede, 2003). Most of these new marsh systems were then historically diked off and used for agriculture. Embankments of some polders have been intentionally breached to restore tidal marsh communities and associated ecosystem services (Wolters et al., 2005).

Recently there has been renewed interest in the creation of tidal wetlands to off-set widespread historical marsh losses (Boorman et al., 2002; Craft et al., 2002). In order for emergent vegetation to become established within the intertidal zone, the substrate of any constructed tidal marsh must be at the correct tidal elevation (Broome et al., 2019). In naturally developed Holocene tidal marshes, this elevation has been achieved by initial accumulation of predominantly clastic material in sheltered low energy environments (Allen, 2000; Long et al., 2006). Void spaces make up much of the volume of the accreted material on marsh platforms (Turner et al., 2000), and decrease with depth due to the mass of overlying material and organic matter degredation (e.g. Allen, 2000; Brain et al., 2017). Marsh sustainability therefore requires that organic and inorganic sediment accretion keep pace with the compounding impacts of sea level rise and sediment autocompaction (Cahoon et al., 1995). Emergent low marsh can quickly build elevation as marsh grasses increase friction, reduce current velocities, and hasten the trapping of allochthonous suspended sediment (Bouma et al., 2005) and suspended particulate organic material (Mariotti et al., 2020). In addition to trapped sediment, marsh grass growth produces autochthonous vegetative material mainly via its roots, further contributing to marsh platform elevation. As the elevation of a marsh platform nears the level of high tide, the duration and depth of tidal inundation decreases. In prograding marshes, the horizontal distance between the high marsh and the marsh edge increases. Over time this reduction in tidal inundation and increased distance to the

89   marsh edge reduces the transport and trapping of suspended sediment, causing in situ organic
90   production to become the main contributor to continued marsh accretion (French and Spencer, 1993).

91   Within the densely developed coastlines of the Northeast US, tidal restoration via the removal of
92   culverts or barriers to tidal circulation is the most common restoration method (Neckles et al., 2002;
93   Warren et al., 2002), with several studies documenting success in replicating natural marsh habitat
94   metrics. Additionally, new marshes have been intentionally created by placing dredge spoils in shallow,
95   sheltered areas (Yozzo et al., 2004). In the US state of South Carolina, low marsh became established on
96   dredge spoils with similar vegetation and faunal assemblages as nearby reference marshes in as little as
97   four years (LaSalle et al., 1991). Other studies have documented similar findings, with restored marshes
98   generally having high ecological index scores (Staszak and Armitage, 2012) and low colonization by
99   invasive species after tidal restoration (Lechêne et al., 2018). These previous field studies have focused
100   on restored extant marshes or intentionally creating new marshes to stabilize dredge spoil piles, and
101   generally rely on observations made within <10 years following restorative action.

102   In contrast to deliberate efforts to create or restore marshes, here we highlight marshes that have been
103   inadvertently created in response to human activity, focused on tidal freshwater marshes developed
104   since the onset of the industrial era within the Hudson River Estuary in New York State, USA. We use
105   sediment cores and historical maps to show that these marshes formed in association with a diverse set
106   of anthropogenic features, including railroad berms, dredge spoil piles, and jetties. Resulting decreases
107   in hydrodynamic energy at these sites allowed for rapid accumulation of clastic sediments and
108   establishment of emergent marsh vegetation. We compare lithologic characteristics of these young
109   emergent marshes with those of a pre-industrial marsh to identify differences in their defining
110   characteristics. Lastly, we detail the stages of marsh development to provide a conceptual model of
111   successful marsh creation, which can be used as reference for tidal marsh restoration practitioners.

112   2. **Site Description**

113   *2.1 Hudson River Estuary*

114   The Hudson River drains a ~38,000 km^2 watershed, with roughly 70% of the freshwater discharge and
115   sediment supplied by the combined contributions of the Upper Hudson (above Troy, NY) and Mohawk
116   Rivers. The remaining 30% of discharge for the lower Hudson is provided by tributaries draining directly
117   into the tidal river below Troy (Panuzio, 1965; Abood, 1974). Mean annual freshwater river discharge at
118   the Battery (river km 0) is 550 m^3 s^{-1}, but is highly seasonal, with annual maxima often occurring during
119   spring snowmelt events (Olsen et al., 1978). The region is micro-tidal, with an average tidal range of
120   roughly 1.2 m. Tides propagate roughly 240 km upriver from the Battery in New York City (river km 0,
121   Fig. 1). The salinity front is generally located in river km 35-100 (between Hastings, NY and New
122   Hamburg, NY), with the landward reach of the tidal river entirely fresh (Ralston et al., 2008). The entire
123   tidal reach is referred to herein as the Hudson River Estuary following common practice (Nitsche et al.,
124   2007). Past estimates of average annual sediment delivery to the estuary have varied, but generally fall
125   within the range of 0.4 to 1.0 Mt yr^{-1} (Ralston et al., 2013). A more recent and thorough estimate places
126   the total sediment delivery to the estuary at 1.2 Mt yr^{-1} (Ralston et al., 2020 PREPRINT).

127   *2.2 Geologic Setting*

128   Steep bedrock shorelines confine the Hudson River for much of its tidal reach, contrasting with the
129   mouths of many large river systems along passive tectonic margins. Pleistocene glaciation
130   overdeepened the valley, with bedrock eroded down as much as 200 m below the present day river
131   surface (Worzel and Drake, 1959). The active river channel fills much of the narrow valley. As a result,

132 there is limited space for tidal marsh development within the estuary (Tabak et al., 2016). In assessing
133 the tidal marsh abundance and spatial distribution within a 2008 dataset (Cornell IRIS, 2011), we find
134 that emergent tidal vegetation covers only 14 km^2, two-thirds of which is located upstream of river km
135 150. For reference, the surface area of the tidal river itself is approximately 300 km^2. The Northeast US
136 generally has low sediment yields relative to global averages due to inactive tectonics and limited relief
137 (Meade, 1982).

138 Humans have altered the region's landscape and consequent delivery of sediment to the Hudson River
139 Estuary. Economic development in the late 1700s and throughout the 1800s drove the construction of
140 hundreds of mill dams on steep tributaries to the Hudson (Bruegel, 2002). However, many of these
141 dams are small and built on natural knickpoints, and as such, only contain in total 2-3 years of typical
142 annual sediment delivery to the estuary (Ralston et al., 2020). New York City developed the Croton River
143 watershed for water supply in the early 1800s, likely reducing this direct sediment supply to the saline
144 estuary. The city expanded to the Catskill watershed of the Rondout, Esopus, and Schoharie rivers in the
145 early 1900s. The Ashokan Reservoir (built 1915) on the Esopus River traps roughly 97% of the sediment
146 from its upstream catchment (Ralston et al., 2020). Deforestation was extensive, with 80-90% removal
147 of old growth forest peaking in roughly 1850 (Kudish, 2000). It remains unclear to what extent
148 deforestation resulted in greater sediment loads, with lake records in neighboring Vermont showing
149 limited impacts (Cook et al., 2015), but sedimentary records in the western Hudson River watershed
150 show a distinct increase in erosion coincident with deforestation (Hilfinger IV et al., 2001). Climate
151 change has generally made this region wetter, resulting in increased flood frequency (Armstrong et al.,
152 2012), which is contributing to increasing erosion and resultant sediment loads (Cook et al., 2015; Yellen
153 and Steinschneider, 2019).

154 Bedrock composition varies along the tidal river, but can generally be lumped into four main
155 physiographic provinces. To the east of the river, the Taconic uplands are characterized by low-grade
156 metamorphic calcareous and micaceous rock units that readily form fine-grained soils. Localized
157 outcrops of high grade metamorphic rocks make up the higher ridges of the Taconics (Faber, 2002).
158 West of the river, much of the watershed falls within the Catskill physiographic province, with bedrock
159 made up of clastic sedimentary rocks, including shales that tend to form fine grained soils (McHale and
160 Siemion, 2014). As a result of fine soil texture and steep slopes, Catskill streams are more prone to high
161 turbidity than surrounding regions (Ahn et al., 2017). Much of the valley floor falls within the Hudson-
162 Mohawk Lowlands, underlain by Cambrian and Ordovician age sedimentary rocks that have been
163 preferentially eroded. Glaciofluvial and glaciolacustrine sediments associated with Glacial Lake Albany,
164 which existed during the retreat of the Wisconsin Ice Sheet, mantle much of the valley floor (Rayburn et
165 al., 2007). In its lower reaches, the tidal river flows through a canyon within erosion-resistant crystalline
166 rocks of the Hudson Highlands, characterized by thin soils (Olsson, 1981).

167 *2.3 Hudson River Anthropogenic Changes*

168 Beginning in the mid-1800s, large-scale projects made several changes to the channel and shorelines of
169 the Hudson River tidal reach. The Hudson River Railroad, completed between 1849 and 1851, runs
170 directly along the east shore of the river, often crossing shallow embayments (Aggarwala, 1993). A
171 competing rail line, The West Shore Railroad, was constructed in segments during the 1860s and 1870s
172 ("Opening the West Shore," 1883), and similarly crosses many shoals between headlands on the west
173 side of the Hudson.

174 Historically the upper estuary channel (river km 190 to 240) was braided and shallow, impeding
175 navigation. The federal government took control of Hudson River navigation projects in 1831,
176 constructing a number of longitudinal dikes to constrict flow and increase scour in the main channel
177 (Collins and Miller, 2012). Additionally, the channel has been actively dredged and deepened since the
178 1800s (Miller et al., 2006). This same dredging and channel deepening increased the tidal range at the
179 head of the estuary by roughly 0.8 m, largely by reducing drag and increasing drainage efficiency, which
180 has served to lower low tides and decrease the magnitude of fluvial flooding (Ralston et al., 2019).
181 Dredging efforts deepened the navigational channel in 1867, 1925, and 1932, resulting in a doubling of
182 channel depths from roughly 10 m to 20 m for much of the Hudson's tidal reach. Within river km 185-
183 241, dredge spoils filled in approximately 13 km^2 of former shallow and intertidal habitat during the
184 20th century (Miller et al., 2006). In 1819 the average channel depth in the upper tidal river was just
185 over 1 m, but since the 1930s, a 9.7 m deep channel has been maintained (Collins and Miller, 2012).
186 Piers cutting across the channel to lighthouses and other features were also constructed throughout the
187 19th and 20th centuries, including the Saugerties lighthouses at the mouth of Esopus Creek, one of our
188 study sites. The majority of these shoreline modifications occurred during an era of reforestation and
189 rapid dam building in the watershed, both of which would have potentially reduced sediment supply to
190 the estuary.

191 *2.4 Study sites*

192 We focus here on five Hudson tidal freshwater wetland complexes associated with significant
193 anthropogenic shoreline alterations (Fig 1). We used sediment cores and historical aerial imagery to
194 reconstruct wetland development, focusing on sediment characteristics, accumulation rates and
195 constraints on the timing of emergent marsh. Three of our sites are in coves bounded by railroad berms
196 that were completed in 1851: Tivoli North Bay, Tivoli South Bay, and Vanderburgh Cove. Each of these
197 sites represents a different stage in wetland development, progressing from open water and tidal flat
198 towards emergent marsh. Tivoli North Bay is completely colonized by marsh, with cattail (*Typha*
199 *angustifolia*) making up the dominant cover. Vanderburgh Cove is 53% open water with the remaining
200 portion made up of emergent cattail marsh (14%) and lower intertidal vegetation (31%), mostly
201 consisting of spatterdock (*Nuphar advena*). Tivoli South Bay is 95% open water, with the remaining area
202 spatterdock (4%) and cattail (1%). Open water areas of all three railroad-bounded coves are dominated
203 seasonally in the summer by invasive water chestnut (*Trapa natans*), which was introduced in 1884
204 (Smith, 1955). Two culverts under the railroad causeway berms allow for tidal exchange from the
205 Hudson to Tivoli North Bay and Vanderburgh Cove, and three culverts connect the Hudson to Tivoli
206 South Bay (black arrows in Fig. 1D and 1F). Small local tributaries also discharge into the three railroad
207 impounded coves, all with similar watershed areas of ~60 km^2 (Table 1).

208 Two additional anthropogenic sites are not significantly impacted by railroad berms and instead remain
209 more open. Stockport Marsh is located in the lee of a large promontory built from dredge spoils, with an
210 associated prograding sand spit protecting the marsh from higher energy conditions. Esopus Marsh, at
211 the delta of the Esopus River, is protected by three radial jetties that were constructed to maintain a
212 tributary navigational channel and to provide access to a lighthouse since 1888 (Ladlow, 2019). Key
213 attributes of all five anthropogenically modified coves and marshes are detailed in Table 1. Finally, a
214 sixth site, Iona Island Marsh, was evaluated as a control, as it has been a marsh since at least 6.8 kya
215 (Chou and Peteet, 2010) due to naturally sheltered conditions behind a bedrock island (Fig. 1E). The

216 West Shore Railroad was constructed across Iona Island in ~1870, but post-dates marsh development as
217 documented in Chou and Peteet (2010), and by historical maps.

218 **3. Methods**

219 *3.1 Sample Collection*

220 Transects of sediment cores were collected from each tidal cove by methods determined by site
221 conditions. At the open-water Tivoli South Bay site, piston push coring conducted at high tide was used
222 to recover 2.2 m overlapping drives. At all other sites, a 6.3 cm diameter gouge corer was used to collect
223 1 m overlapping drives. Both of these coring methods are well suited to recovering uncompacted
224 sediments, such that core depth reflects true depth below grade. When highly porous and fibrous marsh
225 surface sediment caused poor gouge core recovery, a 5 cm diameter Russian peat corer was used to
226 collect 0.5 m long surface drives. At nearly all core sites (see Fig. 1 for locations), successive drives were
227 collected until a resistant stratum below marsh or cove muds was reached. This resistant layer was
228 either sandy mud or massive grey clay visibly devoid of organic material.

229 *3.2 Sample* Analysis

230 Cores were transported to the University of Massachusetts Amherst where they were split, described,
231 and stored at 4°C. Split cores were scanned using an ITRAX x-ray fluorescence (XRF) core scanner with a
232 molybdenum tube running at 30kV and 55mA with ten-second exposure times (Croudace et al., 2006).
233 Similar XRF settings have been employed for past studies on the Hudson and where the relative
234 abundance of XRF-obtained Zn has been shown to be particularly effective in identifying the industrial
235 onset of heavy metals (Brandon et al., 2014).

236 Every 10 cm and above and below visible lithologic transitions we removed a 1 cm thickness subsample
237 for determination of bulk density, percent organic content, and grainsize. Subsamples were weighed
238 wet and dry and then combusted, with change in sample mass calculated after each step to derive water
239 and organic mass from loss on ignition (LOI) following procedures in Dean, (1974), and dry bulk density
240 based on the empirical LOI mixing model described by Morris et al. (2016). Dry bulk densities were also
241 determined independently by assuming water content as a proxy for void space and inorganic and
242 organic densities of 2.4 g cm^{-3} and 1.2 g cm^{-3}, respectively (Neubauer, 2008), which provided similar
243 results but tended to be biased high due to sediments likely not being fully saturated when obtaining
244 wet weight. Burned samples were gently disaggregated with mortar and pestle then run through a
245 Beckman Coulter LS 13 320 laser diffraction particle size analyzer with a range of 0.4 µm to 2000 µm,
246 and sonicated for 15 seconds before measuring the sample for 60 seconds. An alternative digestion
247 method using a double treatment of 30% hydrogen peroxide was also tested, but visual inspection of
248 these processed samples under 100X magnification showed incomplete digestion of organic particles.

249 *3.3 Sediment age constraints*

250 We constrain sediment ages using down-core profiles of short-lived radionuclides via gamma
251 spectroscopy and heavy metal chronologies from XRF core scanning. Visual observation of split cores
252 revealed common stratigraphy discussed below that could be traced across individual transects.
253 Following this visual inspection, one or two representative cores from each marsh transect were
254 selected to obtain additional age constraints via down-core concentrations of ^{137}Cs and unsupported
255 ^{210}Pb. For these short-lived radioisotopic analyses subsamples of 1 cm thickness and approximately 6 g

256 dry mass were counted for at least 48 hr on a Canberra GL2020R Low Energy Germanium Detector. We
257 primarily rely on the 1963 peak in ^{137}Cs as age and 1954 CE onset following methods in Pennington et al.
258 (1973). In cores that displayed decreases in ^{210}Pb with depth, we further constrained sediment ages
259 based on unsupported or excess ^{210}Pb activities, defined as the difference between total ^{210}Pb activities
260 and the in situ supported ^{210}Pb as measured by ^{214}Pb (Chen et al., 2004). Unsupported ^{210}Pb activities
261 were converted to age using methods described by Appleby and Oldfield (1978) assuming a constant
262 initial concentration (CIC) of excess ^{210}Pb. All ^{137}Cs, ^{210}Pb and ^{214}Pb profiles, as well as derived age
263 models, are presented in Ladlow (2019), and the ^{137}Cs and excess ^{210}Pb derived chronologies were
264 generally consistent.

265 The onset of increased heavy metals in cores is linked to the beginning of the industrial era and dates to
266 1850-1900 in the region (e.g. Olsen et al., 1978). Here we employ zinc as a general proxy for heavy
267 metals as it has been shown to have the clearest industrial related onset and least noise among heavy
268 metals evaluated by XRF core scanning (e.g. Brandon et al., 2014). A strong correspondence has also
269 been observed between heavy metal profiles of Zn and Pb (e.g., Benoit et al., 1999), but with a much
270 noisier Pb signal derived from the XRF scanning technique (Ladlow, 2019).

271 Historical maps and aerial photos were used to constrain the timing of anthropogenic impacts at each
272 study site, as well as to track the extent of tidal marsh through time. Topographic maps were accessed
273 from the US Geological Survey's National Geologic Map Database Project. Historical navigation charts
274 were accessed from NOAA's Office of Coast Survey's Historical Map & Chart Collection. Aerial images
275 were accessed via USGS's Earth Explorer application. These data sources were then used to map
276 marshes that have formed within anthropogenic backwaters throughout the entire estuary using a 2007
277 geospatial dataset of the tidal wetland extent along Hudson River (Cornell IRIS, 2011).

278 **4. Results**

279 *4.1 Tivoli North Bay*

280 Our sampling of Tivoli North Bay (TVN) was composed of a west-to-east transect of five cores across the
281 marsh surface (Fig. 1F). The transect began at TVN2 collected 110 m from a north-south oriented tidal
282 channel that runs directly behind the railroad berm, followed west-to-east by TVN3, TVN1, TVN4 and
283 TVN5 (Fig. 1), with the TVN5 core collected 10 m from the edge of another, larger tidal channel that runs
284 along the landward side of the marsh. This landward tidal channel also serves as the fluvial outlet of
285 Stony Creek, a small tributary that drains a local watershed of 55 km^2.

286 We observed an abrupt up-core decrease in median grain size, from 20-40 μm to less than 10 μm for a
287 majority of cores in the transect (Fig. 2). For the four most eastern cores (TVN3, TVN1, TVN4 and TVN5),
288 this onset to finer grained deposition occurred at a depth of between 160 and 170 cm, and shallowed to
289 a depth of roughly 135 cm in the most western TVN2 core. A gradual, and then more pronounced
290 increase in organics is observed above the sharp coarse-to-fine grained transition, with the transition to
291 greater organic fractions at a depth between roughly 70 and 90 cm, increasing from approximately 10%
292 LOI below to 35% LOI above. We observe this prominent surficial increase in organics for all cores except
293 TVN5, where organics are observed to increase but remained below 20% LOI.

294 Chronological markers from zinc onset, ^{137}Cs, and ^{210}Pb inform a depth-to-age model for Tivoli Bay North
295 (Fig. 3). The zinc profile for TVN3 in the upper 50 cm of the core was relatively noisy due to highly
296 porous organic sediments and root matter. Below this surficial unit, an initial rise in zinc is observed at
297 roughly 150 cm. The ^{137}Cs depth profile for the same core reveals a 1954 CE onset in detectable activity

298   above 60 cm, followed by a 1963 CE peak at 35 cm. We also isolated the 1954 CE ^{137}Cs onset in core
299   TVN4 to a similar depth of 61 cm, suggesting consistent deposition rates between cores (Fig. 2). We
300   observed a general increase in total ^{210}Pb activities towards the surface in TVN3, with the exception of
301   two samples counted between 20 and 40 cm. Supported ^{210}Pb, as defined by Pb-214 activities, remained
302   relatively uniform downcore in TVN3, indicating that trends in overall ^{210}Pb activity likely also reflect
303   variability in unsupported ^{210}Pb. ^{210}Pb-derived ages for TVN3 are not all chronologically consistent due to
304   drops in activity between 20-40 cm. However, the best fit to unsupported ^{210}Pb derived ages results in a
305   deposition rate of 0.9 cm/yr, which is consistent with independent accumulation rates based on the
306   1954 onset of ^{137}Cs and the industrial onset of zinc assuming a common age of 1850 CE corresponding to
307   railroad construction. A derived deposition rate of 0.9 cm/yr for TVN3 dates the 165 cm lithologic
308   transition to finer sediments in the core to the early-to-mid 1800s (Fig. 2). This rate is similar to, yet
309   somewhat higher than, the range of 0.7-to-0.8 cm/yr obtained to the south of our transect in marshes
310   fringing Cruger Island by Sritrairat et al., (2012) (white squares in Fig 1F).

311

312   *4.2 Tivoli South Bay*

313   Tivoli Bay South (TVS) is separated from Tivoli Bay North by a tombolo that extends from the eastern
314   shore of the Hudson River to the bedrock outcrop that forms the center of Cruger Island (Fig. 1). In
315   contrast to expansive tidal wetlands in Tivoli Bay North, Tivoli Bay South is predominantly tidal flats,
316   with just a thin strip of emergent wetlands that flank its mainland shore. Similar to Tivoli Bay North, the
317   west side of the bay is now defined by a railroad berm, through which three culverts serve as the
318   primary tidal connections between the bay and the main Hudson River. An additional side tributary
319   (Sawkill Creek), empties into to Tivoli Bay South to the east, draining a watershed of approximately 68
320   km^2.

321   Three cores were collected along a west-to-east transect (Fig. 1F), spanning the widest part of the bay
322   and terminating 210 m away from the mouth of Sawkill Creek. We observed a sharp drop in median
323   grain size in all three of these cores at varying depths (Fig. 4), similar to observations from Tivoli Bay
324   North cores (Fig. 2). The up-core decrease in D$_{50}$ was most apparent at the western TVS1 core, where at
325   roughly 120 cm the median grain size decreased from 40 μm to less than 4 μm. In TVS2 and TVS1 this
326   drop in grain size occurred at shallower depths of 117 cm and 59 cm, respectively. The drop in grain size
327   in TVS2 was smaller in magnitude than TVS1, decreasing from about 20 μm to 10 μm. Conversely, we
328   observed a larger drop in grain size at TVS3, decreasing up-core from >200 μm to 20 μm. All cores from
329   TVS showed a gradual rise in zinc just above their respective step-function drops in grain size, while
330   organic content throughout these cores remained relatively low at roughly 5% LOI.

331   We observed a 1954 CE onset and 1963 peak in ^{137}Cs activity in TVS1 at roughly 40 cm and 35 cm,
332   respectively (Fig. 4). Farther down in TVS1, the onset for ~1850 industrial-derived zinc began at 95 cm
333   (Fig. 4). A complete depth profile of ^{210}Pb was not obtained from TVS1; however, ^{137}Cs and zinc-derived
334   ages are all consistent with an average deposition rate at TVS1 of 0.6-to-0.7 cm yr^{-1}. We find this rate
335   consistent to previous ^{137}Cs-derived accumulation rates from Tivoli South Bay of 0.59, 0.60, 0.68, 0.77
336   and 0.93 cm yr^{-1} presented by Benoit et al. (1999), but less than their average 1.16+/- 0.3 cm/yr when
337   including rates derived from ^{210}Pb. Our ^{137}Cs-derived deposition rate of 0.65 cm/yr at TVS1 resulted in an
338   approximate age for the core's grain-size transition at 120 cm of sometime between the early-and-mid
339   1800s, which was similar to the age obtained for the same transition at TVN3 and consistent with the
340   timing of railroad construction at both sites.

341

342   *4.3 Vanderburgh Cove*

8

343   We collected two transects of cores from Vanderburgh Cove (see Fig. 1 for core locations). A transect
344   across the emergent marsh began at core site VBM3 near the tributary mouth of the Landsman Kill
345   (watershed area of 61 km^2), and progressed south to the center (VBM2), and distal edge (VBM1) of the
346   marsh. A second Vanderburgh transect crossed the open-water tidal flat area of the cove beginning near
347   the marsh edge (VBC4) and extending south to the center (VBC5) and southeastern side (VBC6) of the
348   cove.

349   Within core VBM1, we observed zinc onset and a concurrent grain size transition at a depth of 167 cm
350   (Fig. 5), which is similar to the depth observed at Tivoli North. At 75 cm depth, the onset of leaf
351   fragments was noted in visual observations. Rootlets were evident from 53 cm upward to the surface,
352   likely indicating the transition from intertidal mudflat to marsh, and supported by a gradual increase in
353   LOI to ~10% at the surface. VBM2 and VBM3 were less than 150 cm in length, with core recovery
354   impeded by refusal in sandy material at that depth. This sandy material likely represented coarse deltaic
355   deposits from Landsman Kill. Neither VBM2 nor VBM3 displayed a zinc onset or a transition in grain size
356   (Fig. 5). VBM2 and VBM3 displayed generally greater organic contents than observed at VBM1, likely
357   due to the rapid horizontal expansion of tidal wetlands at VBM1, as observed in historical aerial photos
358   (Supp. Fig. 1). Historical aerial photos suggest that marsh at Vanderburgh did not emerge until after
359   1978. The marsh's position at the mouth of Landsman Kill and its recent emergence contrast with marsh
360   development at Tivoli North, for which there is no evidence of marsh development beginning at a
361   tributary mouth. In turn, at Vanderburgh we consider ^{137}Cs-derived ages as a better representation of
362   wetland accretion rates than ages derived from the earlier zinc onset. For the VBM1 marsh core we
363   observe the 1954 CE onset and subsequent 1963 CE peak at respective depths of 94 cm and 90 cm (Fig.
364   5). These ^{137}Cs age constraints result in marsh accretion rates of 1.5-1.6 cm yr^{-1}, much greater than the
365   rate of 0.9 cm yr^{-1} obtained at Tivoli North Bay's marsh (Fig. 3).

366   Open water cores from Vanderburgh (VBC4-VBC6) all exhibited concurrent onsets in zinc and decreases
367   in grain size similar to VBM1, at 112 cm, 133 cm, and 104 cm respectfully. Above this transition, median
368   grain size was between 8 and 14 μm (fine silt) for all Vanderburgh cores with the exception of surface
369   material in VBM2 and VBM3 (Fig. 5). Similar to Tivoli Bays, we interpret the drop in grain size in the
370   VBC4-VBC6 cores as marking the timing of railroad construction in 1851 CE (Fig. 5), which results in
371   subsequent accumulation rates of 0.6 to 0.8 cm yr^{-1}. If the lithologic transition at 167 cm in VBM1 also
372   represents railroad construction, we obtain an accumulation rate of 0.7 cm yr^{-1} for the interval below
373   that 1954 onset for ^{137}Cs, a rate similar to that observed in the open water portions of the cove.

374   *4.4 Stockport Marsh*

375   A series of nautical charts and aerial images from the twentieth century help to illustrate wetland
376   development at the Stockport Marsh site. A nautical chart from 1915 shows that a delta extended west
377   from the mouth of Stockport Creek approximately 200 m, with a total areal extent of 5x10^4 m^2 (US Coast
378   and Geodetic Survey, 1915). South of Stockport Creek's mouth, a < 1 m deep shoal extended out
379   approximately 600 m from the shore with no denotations for marsh. Nautical charts from 1929 indicate
380   no significant change to this morphology (US Coast and Geodetic Survey, 1929). However, in 1930 a 6
381   x10^4 m^2 island appeared at the western edge of the shoal directly to the west of Stockport Creek's
382   mouth and grew to 1.9 x10^5 m^2 by 1932 (Fig. 6A). A 1953 topographic map indicates that much of this
383   island was more than 3 m above sea level at that time, similar to its present elevation. The abrupt
384   appearance of this feature and its elevation well above that of natural deltaic deposition suggest that
385   dredge spoil emplacement created this island, which is consistent with the timing of major navigation
386   improvements here during the late 1920s and early 1930s (Miller et al., 2006). By 1960, an aerial photo
387   shows a spit extending southward from the dredge pile along the shallow shoal depicted in navigational

388 charts (Fig. 6B). The embayment formed by this spit remained mostly open water in 1960. Conversely, a
389 1978 aerial photo shows that abundant emergent vegetation had developed during the 18 years that
390 had elapsed since 1960 (Fig 6C).

391 We analyzed a north-to-south transect of cores from Stockport Marsh, with the most northern SPM7
392 nearest to the dredge spoil island, SPM4 in the center of the marsh, and SPM1 nearest to the southern
393 edge of the marsh and 4 m away from a major tidal channel (Fig. 1). The sand-to-mud transition was
394 most abrupt in SPM4 at approximately 95 cm (Fig. 7), with more gradual transitions in SPM7 and SPM1
395 centered at approximately 75 cm and 115 cm, respectively. SPM7 and SPM4 exhibited similar increases
396 in organic content above their respective sand-to-mud transitions, reaching peak values of ~40% LOI
397 near the surface. The increase in organics was less evident closest to the marsh edge in SPM1, which is
398 consistent with lower organic content in marsh edge observations from VBM1 (Fig. 5) and TVN5 (Fig. 2)
399 and other studies of tidal marsh organic content (Palinkas and Engelhardt, 2016; Temmerman et al.,
400 2003).

401 Depth profiles of ^{137}Cs from the center of the marsh (SPM4) identified a 1954 CE onset and 1963 CE peak
402 at roughly 55 cm and 35 cm and respective average deposition rates of 0.9 cm/yr and 0.7 cm/yr. [1] At the
403 marsh's southern edge (SPM1), the 1954 CE onset and 1963 CE peak in ^{137}Cs was observed at depths of
404 106 cm and 61 cm, with respective deposition rates of 1.7 cm/yr and 1.1 cm/yr. This discrepancy in
405 calculated deposition rates from ^{137}Cs onset (1954) to peak (1963) is consistent with rapid trapping of
406 fine-grained sediment resulting from the concurrent development of the sand spit. Depth profiles of zinc
407 from the SPM cores exhibited significant noise and data gaps; however, the onset for zinc in SPM7
408 appears to be deeper than the sand-to-mud transition (Fig. 7), which is also consistent with the sand-to-
409 mud transition in SPM7 dating to the ~1930 emplacement of dredge spoils, well after industrial activity
410 introduced heavy metals to this region.

411 *4.5 Esopus Marsh*

412 The Esopus marsh/delta complex lies on the western side of the Hudson River approximately three
413 kilometers north of Tivoli Bays (Fig. 1). Esopus Creek drains a 1100 km^2 watershed with sub-catchments
414 known for higher-than-regional-average sediment yields (Ahn et al., 2018). Dredging began at the mouth
415 of the Esopus in 1888, with jetties built on either side of the navigation channel to prevent shoaling
416 ("Timeline – Saugerties Lighthouse," 2011). An 1863 nautical chart shows shoals in the areas to the
417 north and south of these jetties that is now occupied by marsh. Historical maps are consistent with
418 marsh development following jetty construction (Fig. 8).

419 We obtained a series of five cores from the Esopus Marsh complex including four to the south of the
420 jetty-hardened channel (ESP1-ESP4) and one to the north (ESP5). The grain size profile from ESP3 reveals
421 a sand-to-mud transition at ~85 cm that is concurrent with the onset in zinc (Fig. 9). We observe a
422 gradual rise in organic content above this sand-silt transition that begins below 3% LOI and rises to
423 values that range between 9 and 13% above a depth of 65 cm. Activities of ^{137}Cs at ESP3 reveal a 1954
424 CE onset near the base of this greater organic content unit at ~60 cm, followed by a subsequent 1963 CE
425 peak at 50 cm. [137]Cs age constraints from two cores both provide an approximate accumulation rate of
426 ~0.9 cm/yr for recent marsh material.

427 Grain sizes for ESP1 and ESP2 were not obtained, however, LOI profiles for these cores revealed a similar
428 ~80 cm rise in organics as that observed in ESP3 (Fig. 10), as well as a concurrent rise in zinc. In the two

429   cores that are closest to the Esopus channel (ESP4 and ESP5), we observed a deeper zinc onset and
430   increased LOI at ~120 cm. We find that a higher rate of deposition at ESP5 based on zinc onset depth is
431   consistent with ^{137}Cs activities obtained for the core, where the 1954 onset and 1963 peak were
432   observed at ~94 cm and 80 cm, respectively (Fig. 10). The resulting ^{137}Cs-derived accumulation rate for
433   ESP5 is roughly 1.5 cm/yr. The organic content within surficial sediments at ESP5 was also the highest of
434   all cores collected from the site, with LOI ranging between 20-30% above a depth of ~40 cm.

435   *4.6 Iona Island Marsh*

436   Iona Island is located on the western side of the Hudson and shelters a large wetland complex to its
437   southwest, with 0.49 km^2 of *Typha* and *Phragmites* marsh. Low salinity at Iona Island Marsh of 1-2 ppt
438   on average (Yozzo et al., 2005) suggests limited influence of salinity-driven sedimentation processes
439   such as flocculation (Sholkovitz, 1976). A railroad crosses the island, with earthen berms extending north
440   and south. A 25 m culvert allows for tidal exchange through the southern berm and a 250 m trestle
441   supported by piers traverses the northern entrance.

442   Chou and Peteet (2010) recovered a core from the most sheltered portion of Iona Island Marsh that
443   showed peat down to 9 m with ^{14}C dates from marsh rhizomes placing marsh development there at
444   least by 6.8 kya. We collected a transect of cores from the less sheltered portion of the marsh to
445   evaluate changes in development and lithology following railroad construction (INA1-INA7; see Figure 1
446   for locations). We observed the 1954 onset of ^{137}Cs at 15 cm in INA5 and obtained a resulting deposition
447   rate of 0.23 cm/yr. The ~1850 CE onsets for zinc in INA cores were observed between 35 and 45 cm,
448   consistent with relatively slow and uniform deposition rates throughout the marsh of between 0.2 and
449   0.3 cm/yr (Figure 11). These vertical accumulation rates are 3-5 times less than those observed at our
450   other study sites, which is consistent with pre-industrial development of Iona Island Marsh and slower
451   accretion rates controlled by sea level rise. Organic content of the peat here was typically greater than
452   50%, with the exception of INA1, which was located adjacent to a major channel (Figure 11). The
453   inorganic fraction of material in all cores was comprised predominantly of silt, with median grain sizes
454   (D_{50}) generally between 5 μm and 20 μm. We observed no discernable changes in the organic fraction or
455   grain size at the zinc onset, unlike other railroad causeway sites (TVN, TVS, and VBM), where zinc onset
456   provided a regionally consistent proxy for the timing of railroad construction.

457   4.7 *Extent of Anthropogenic Marshes on the Hudson*

458   Given the stark contrasts in old versus anthropogenic marshes, and the sediment needs of rapidly
459   developing anthropogenic marshes, we mapped tidal marshes that have formed during the industrial
460   era to evaluate their aggregate impact on the sediment budget of the Hudson River Estuary. Beginning
461   with a high resolution geospatial data set of Hudson tidal wetlands (Cornell IRIS, 2011), we identified
462   those marshes that formed since ~1900. We used several data sets to identify past alterations to the
463   river and resultant marsh development including navigational charts, air photos, and topographic maps.
464   Using these historical resources, we estimate that 52% of marshes have developed in the shelter of
465   dredge piles, dikes, jetties, and railroad berms since the mid-1800s. This is a conservative estimate, as
466   only those marshes that were clearly documented as newly extant were classified as anthropogenic.
467   Anthropogenic marshes have disproportionately fostered non-invasive *Typha* marsh, rather than
468   *Phragmites*, with two thirds of all cattail marsh on the Hudson occurring within anthropogenic settings
469   (Supp. Fig. 3).

470 Most new marsh area since the mid-1800s has formed in the upper reaches of the tidal river between
471 river km 193 and 240, largely as a result of early 20th century dredging and longitudinal dikes that
472 transformed the formerly braided upper channel into a single, deeper navigational channel (Squires,
473 1992; Miller et al., 2006; Collins and Miller, 2012). A variety of tidal wetland types have colonized
474 resultant braid channel cut-offs that provided shallow, low-energy environments.

475

476 **5.Discussion**

477 *5.1 Contrasting new and old marshes and tidal flats*

478 We group our field sites into three representative categories: (1) anthropogenic marshes that developed
479 in response to human alterations (Tivoli North, Vanderburgh Marsh, Esopus, Stockport); (2) human-
480 modified coves that remain tidal mudflat with open water at high tide (Tivoli South and Vanderburgh
481 Cove); and (3) natural marsh systems established prior to human alterations (Iona). For these categories
482 we compiled values for observations of organic content, grain size, vertical accumulation rates derived
483 from ^{137}Cs and zinc onset chronologies, and mineral accumulation rates in mass per unit area per time.
484 The number of cores for each site ranged from three to five, and therefore, accumulation rates should
485 be viewed with some caution in accordance with the sample size. For each site, we present average
486 values of all measurements from 0-to-50 cm (Fig. 12), as this depth interval was observed to best
487 capture elevated organics at marsh locations (e.g. Fig. 2, 5,7, and 10) and is consistent with analyses
488 used elsewhere to compare tidal marsh organic content (Morris et al., 2016).

489 Iona Island Marsh, which was established > 6kya (Chou and Peteet, 2010), exhibits the lowest rates of
490 vertical accretion ranging between 0.2 and 0.3 cm/yr (Fig. 12A), consistent with this marsh remaining in
491 step with 20th century regional rates of sea level rise (Kemp et al., 2017). Iona accumulation rates are
492 also similar to those published previously for regional marshes thought to be in steady state with sea
493 level rise (Fig. 13), including Piermont Marsh (0.29 cm/yr in Pederson et al., 2005) and Jamaica Bay (0.32
494 cm/yr in Peteet et al., 2018). Of all our study sites, the slowly accumulating Iona Island Marsh had the
495 greatest organic content, with an average LOI in the top 50 cm of 50% (+/-18%). Organic content for
496 Iona was similar to that published previously from Piermont Marsh (37% +/- 9%, Pederson et al., 2005),
497 and somewhat lower than that published from Jamaica Bay marsh (61% +/- 9%, Peteet et al., 2018).

498 Accumulation rates for the anthropogenic marsh category were typically around ~0.9 cm/yr, 3-4 times
499 greater than those observed in Iona Island Marsh (Fig. 12). Organic content in anthropogenic marshes
500 was also substantially lower than the Iona site, with average LOI values of 10-30% (Fig. 12B). Compared
501 to anthropogenic emergent marshes, human-modified coves (Vanderburgh and Tivoli South) exhibited
502 somewhat slower accumulation rates, averaging between 0.6 and 0.7 cm/yr, but were still 2-3 times
503 greater than rates of accumulation at Iona Island Marsh. Cove sediments also contain the least organic
504 matter, with average LOI in the uppermost 50 cm typically below 10%. At all sites, we observed
505 predominantly silt-size clastic deposition, with median grain sizes between 5 and 20 µm, and no clear
506 grain size delineations between marsh/cove categories (Fig. 12C).

507 The three categories of field site presented here (old marsh, new marsh, intertidal mudflat) display clear
508 differences in their rates of vertical accumulation and mineral sediment storage. We observe
509 approximately 0.3 cm yr^{-1} greater rates of accumulation in anthropogenic marshes than in the
510 anthropogenic coves. This 0.3 cm yr^{-1} discrepancy is similar to the total accumulation rate at pre-

511   industrial Iona Island Marsh. Iona Island Marsh has accreted largely through in-situ production of
512   organic material, as indicated by its high organic content and relatively low rate of mineral accumulation
513   (Fig. 12D). This is largely due to its maturity and high platform tidal elevation, which is known to reduce
514   mineral sediment introduction (Allen, 2000; Darke and Megonigal, 2003). Results therefore support
515   increased accumulation rates of anthropogenic marshes versus coves, being due to the tendency for
516   marsh to build elevation via the combination of clastic sediment trapping and in-situ organic production.
517   Anthropogenic open-water coves appear to trap more inorganic clastic sediment than their
518   anthropogenic marsh counterparts (Fig. 12D). This is consistent with observations from polders, where
519   inorganic sedimentation prior to emergent vegetation establishment can far exceed that observed on
520   vegetated marsh platforms due to greater tidal inundation and accommodation space within newly
521   sheltered intertidal mudflats (Hofstede, 2003). The exception to this is the most recently developed
522   fringing marsh at Vanderburgh Cove (VBM1), where average mineral accumulation rates of between 0.5
523   and 0.6 g cm^{-2} yr^{-1} are similar to those observed within open-water regions of the cove (VBC), and the
524   open-water Tivoli South Bay (TVS) site. Successive aerial photos show that this fringing marsh has
525   developed rapidly since 1978 (Supp. Fig. 1). In contrast, we observe the lowest rate of mineral
526   accumulation among the anthropogenic marshes at Tivoli North Bay (TVN, 0.2 g cm^{-2} yr^{-1}). Tivoli North
527   Marsh (TVN) is also the earliest established of our anthropogenic marshes, with 1932 topographic maps
528   showing similar marsh extent to today (Supp. Fig. 2). It is therefore likely that Tivoli North Marsh has
529   accreted sufficiently that high trapping rates of incoming suspended sediment are limited to marsh
530   locations proximal to channels, and that in-situ organic production accounting for the bulk of accretion
531   in much of the marshes' interior. Median mineral accumulation rates for the less sheltered Esopus (ESP)
532   and Stockport (SPM) marshes are both ~0.3 g cm^{-2} yr^{-1}, which is less than observed in the most recently
533   developing Vanderburgh marsh system, and greater than rates for the more established marshes at
534   Tivoli North.

535   We can apply a basic model that assumes average clastic sediment accumulation rates of 0.3 g cm^{-2} yr^{-1}
536   for anthropogenic marshes and 0.6 g cm^{-2} yr^{-1} to anthropogenic tidal flats to derive a rough
537   approximation of annual net inorganic sediment trapping (i.e. total deposition minus erosion) within
538   these modified areas. While this is a simplification that does not account for heterogeneity of marsh
539   accretion beyond that captured by our core transects, it gives a rough appraisal of the role of sediment
540   storage within post-industrially developed marshes. We approximate 0.07 Mt yr^{-1} of net clastic
541   accumulation in newly developed marshes based on these simplifications, which is equivalent to roughly
542   6% of the present Hudson River sediment load (Ralston et al., 2020).

543   5.2 *Conceptual Model of Marsh Creation*

544   Efforts to create or restore marshes are hampered by the decadal timescales required to evaluate the
545   success or failure of projects. While several studies have documented deleterious effects to extant
546   marshes from hydrodynamic alteration (e.g., Delgado et al., 2013) , we know of no other study that
547   documents the widespread and inadvertent creation of tidal marsh via such human actions. However,
548   there is a growing appreciation for marsh expansion in the Northeast US following European
549   colonization in the 1600s (Braswell et al., 2020).

550   Sediment core data and historical maps and aerial photos from the sites presented here provide
551   examples of the developmental stages from shallow embayment to mudflat to emergent marsh. These
552   observations can be a resource for ongoing and future marsh creation projects, which can be monitored
553   and modified as needed based on comparison with these historical, if inadvertent, successes in marsh
554   creation. For example, the anthropogenic marsh observations presented here provide bounds for
555   expected clastic and organic sediment accumulation rates during marsh creation and development.

556 These results highlight that rapid wetland development is possible even under micro-tidal conditions
557 and in a post-glacial region generally considered to exhibit relatively low sediment yields. The onset and
558 development of marshes in the Hudson in the late 19th and early 20th century coincided with a period of
559 reforestation across the Northeast US (Foster, 1992; Kudish, 2000) and dam construction. Dredging and
560 channelization of the Lower Hudson's tidal channel reduced flooding from discharge events (Ralston et
561 al. 2019). These factors likely reduced sediment inputs to the estuary and delivery to the wetlands, and
562 yet marsh growth was extensive and rapid.

563 Using the anthropogenic marshes at Stockport and Tivoli North as representative cases, we characterize
564 the phases of marsh development at each of these sites. Prior to anthropogenic shoreline changes,
565 shallow, subtidal sand shoals occupied these locations (Sritrairat et al., 2012). The water depths under
566 pre-anthropogenic alterations were likely relatively stable, with deposition of coarse sediment from the
567 Hudson and local tributaries balanced by increased accommodation space due to long-term sea level
568 rise and erosion during periods of elevated wind, tidal energy, and river discharge. The emplacement of
569 dredge spoils at Stockport and railroad construction at Tivoli reduced the hydrodynamic energy within
570 the newly protected coves at each site. This transition in energy conditions was marked by a fining of
571 the depositional sediment, an increase in clastic sediment accumulation rate, and a modest increase in
572 accumulation of particulate organic material. Flood-dominant tidal fluxes from the Hudson River into
573 these coves (Benoit et al., 1999), provided abundant clastic sediment to allow for rapid aggradation of
574 the bed during this phase, which likely resembled low intertidal habitat present today at Vanderburgh
575 Cove (e.g. VBC4). It is worth emphasizing that this phase of aggradation is a key step in the subsequent
576 establishment of emergent marsh vegetation, which has a narrow range of tidal elevation at which it can
577 establish (Odum, 1988; Redfield, 1972). For example, in 2014 lidar data at Vanderburgh Cove, the
578 interquartile range of the elevation (NAVD88) of the boundary between horizontally expanding
579 emergent marsh and low intertidal vegetation (e.g. *Nuphar advena*) is 0.05 to 0.13 mASL (NOAA 2014),
580 which reflects the lower end of the elevation range at which *Typha* begins to colonize at this site. For
581 reference, mean high water is 1.2 mASL at Turkey Point tide gauge (NOAA 8518962), 16 km landward
582 from this site.

583 Over decades, clastic sediment accumulation decreased water depth and allowed for establishment of
584 shallow intertidal vegetation such as *Nuphar advena*, which has roots and corms that contribute to
585 further aggradation of the substrate. Abundant *Nuphar* corms were observed in core VBC4 at
586 Vanderburgh Cove. Cores from marshes showed increased rootlet density characteristic of the transition
587 to emergent marsh and colonization by *Typha* and associated vegetation. A schematic diagram of this
588 mature stage of transition is presented in Fig. 14 showing the roles of human-made structures in
589 reducing hydrodynamic energy and tides in delivering sediment to these sheltered areas. Root density in
590 split cores and LOI indicate the onset of emergent tidal marsh. Root density increased above 100 cm
591 depth in cores from Tivoli North and dated to approximately 1910, compared to a depth of 40 cm at
592 Stockport Marsh and a corresponding age of approximately 1975 based on aerial photographs and [137]Cs
593 chronology (Fig. 6 and Fig. 7). The discrepancy in root onset depth reflects the relative maturity of these
594 two systems and with Stockport Marsh being younger and at a lower elevation in the tidal frame (Supp.
595 Fig. 4).

596 Core locations were not surveyed relative to a global datum, but available lidar data provides a means to
597 evaluate differences in elevation between Tivoli and Stockport. Lidar data suffers from inaccuracy in
598 dense marsh vegetation (Buffington et al., 2016). We evaluated offsets between survey-derived and
599 lidar-derived elevations of the marsh platform at 26 points in Tivoli North Bay. We found a 0.30 m offset
600 (standard deviation = 0.09 m), with lidar values higher than surveyed elevations due to dense vegetation
601 impeding lidar penetration and reflection. Uncorrected lidar-derived elevation values along core

transects yielded a median elevation of the marsh platform at Tivoli North of roughly 1.25 mASL, versus 0.75 mASL at Stockport Marsh (NYSDEC, 2012; Supp. Fig. 4). Assuming that the lidar versus surveyed offset is similar at both marshes, Stockport Marsh is roughly 0.5 m lower than Tivoli North, reflecting its more recent transition from mudflat to marsh. It continues to rapidly trap clastic sediment at twice the rate observed at Tivoli North (Fig. 12), and therefore is more representative of a mineralogenic marsh (Allen, 2000). Conversely, Tivoli North Marsh has accreted sufficiently to reduce tidal inundation at its interior and has transitioned to a more organogenic and mature marsh.

5.3. *Estuarine tidal versus terrigenous fluvial sediment supply*

Most of the sites in this study were located at tributary mouths, raising the question to what extent marshes source their sediment from the main body of the estuary versus a local fluvial source. Benoit et al. (1999) found that tidal sediment contributions from the Hudson over four tidal cycles at Tivoli South Bay were only able to explain roughly 30% of their averaged rate of Pb-210-derived accumulation rates there. However, this percentage increases to roughly 55% when applying our more recent ^{137}Cs derived and slightly lower accumulation rates of 0.6 cm/yr, and 100% when applying earlier average flood-dominated Hudson contributions to Tivoli South Bay measured over eight separate tidal cycles by Goldhammer and Findlay (1988).

Using a regional value for watershed sediment yield of 60 T km^{-2} yr^{-1} (Ralston et al., 2020 PREPRINT) we estimate the likely sediment discharge of Sawkill Creek to TVS since the railroad partially enclosed the cove in 1851. This approach suggests that Sawkill Creek could account for up to 65% of the sediment that has accumulated in Tivoli South Bay if all of the watershed's sediment were trapped within the cove. Perfect trapping is unlikely considering that storm flows deliver a disproportionate amount of sediment, and storm flows have low residence time in side embayments, with reduced sediment trapping efficiency. Therefore, tidal delivery of sediments from the Hudson's main stem to the cove likely supplies most of the accumulated sediment. The range of solutions to this two end-member problem suggests that further study is needed to deconvolve the relative importance of local terrestrial-derived versus estuarine sediment in wetland accretion. However, successful marsh establishment at Stockport Marsh, where there is no direct input of tributary sediment suggests that the estuary alone provides sufficient sediment inputs to rapidly develop emergent tidal wetlands in the Hudson.

It is possible that average rates of deposition over the last few decades via ^{210}Pb and ^{137}Cs chronologies could over predict current rates of trapping at sites like Tivoli South Bay, since current trapping efficiencies for its predominantly tidal flat conditions are potentially less than infilling rates when depths were significantly greater. Analogously, the dredged channels of Jamaica Bay have average rates of infilling since the 1954 ^{137}Cs onset of 1.4 to 1.6 cm/yr (Bopp et al., 1993), more than twice that observed in the shallower, predominantly tidal flat environments of Tivoli South and Vanderburgh Cove (Fig. 13). These enhanced rates of trapping in dredged channels of Jamaica Bay starkly contrast with the five times slower rates of accumulation on the neighboring marsh platform the Jamaica Bay Marsh, where organic content is also higher (Fig. 13). Increased trapping in dredged channels of Jamaica Bay likely contributes to the reduced sediment supply for marshes there that has resulted in lateral erosion and marsh loss in recent decades (Hartig et al., 2002). This is in stark contrast to results presented herein from anthropogenic marshes on the Hudson, which have either remained stable or grown in extent over the same interval. High accumulation rates within these anthropogenic tidal marshes reflect their more recent and rapid development from lower elevations. Longer duration hydroperiods, sheltered conditions, and a readily available sediment supply have allowed them to accrete rapidly towards equilibrium with modern sea level.

Conclusion

We used sediment cores and historical evidence from maps, charts, and aerial photos to reconstruct the developmental histories of six tidal wetland complexes in the Hudson River Estuary. Five of the sites are representative of a suite of anthropogenic shoreline modifications that are widespread in the tidal river, especially in its uppermost 100 km. Iona Island Marsh was used as a reference site, as emergent marsh there long predates industrial modification of the Hudson's channel and coastlines. We found that newly sheltered anthropogenic marshes and coves accumulate clastic sediment up to 10-30 times faster than the long-established reference site. A geospatial analysis of all extant wetlands in the Hudson River Estuary indicated that more than half of the emergent marsh has grown in the last ~120 years, with an estimated net clastic sediment accumulation that constitutes roughly 6% of the annual suspended sediment load for the Hudson. Anthropogenic wetland/cove sites represent different phases of emergent marsh development, including tidal mudflat (e.g. Tivoli South Bay), rapidly growing tidal marsh (e.g. Vanderburgh and Stockport Marshes), and mature marsh (e.g. Tivoli North Bay). Together, these sites offer examples of expected environmental transitions for future tidal marsh creation projects. The work also helps to highlight that freshwater tidal wetlands can be created relatively quickly along micro-tidal estuaries in regions generally considered to have low sediment delivery to the ocean similar to the Hudson River in the Northeast US.

Data Availability Statement

Data from sediment cores that were collected in association with this manuscript are archived here: https://doi.org/10.7275/dh3v-0x33

CITATIONS

Abood, K.A., 1974. Circulation in the Hudson Estuary. Annals of the New York Academy of Sciences 250, 39–111. https://doi.org/10.1111/j.1749-6632.1974.tb43895.x

Ahn, K.-H., Steinschneider, S., 2018. Time-varying suspended sediment-discharge rating curves to estimate climate impacts on fluvial sediment transport. Hydrological Processes 32, 102–117. https://doi.org/10.1002/hyp.11402

Ali, L., 2002. An integrated approach for the improvement of flood control and drainage schemes in the coastal belt of Bangladesh. CRC Press.

691   Allen, J.R.L., 2000. Morphodynamics of Holocene salt marshes: a review sketch from the Atlantic and
692   Southern North Sea coasts of Europe. Quaternary Science Reviews 19, 1155–1231.
693   https://doi.org/10.1016/S0277-3791(99)00034-7
694   Appleby, P.G., Oldfield, F., 1978. The calculation of lead-210 dates assuming a constant rate of supply of
695   unsupported 210Pb to the sediment. Catena 5, 1–8.
696   Armstrong, W.H., Collins, M.J., Snyder, N.P., 2012. Increased Frequency of Low-Magnitude Floods in
697   New England1. JAWRA Journal of the American Water Resources Association 48, 306–320.
698   https://doi.org/10.1111/j.1752-1688.2011.00613.x
699   Benoit, G., Wang, E.X., Nieder, W.C., Levandowsky, M., Breslin, V.T., 1999. Sources and history of heavy
700   metal contamination and sediment deposition in Tivoli South Bay, Hudson River, New York.
701   Estuaries 22, 167–178.
702   Biggs, D.A., 2012. Quagmire: Nation-building and nature in the Mekong Delta. University of Washington
703   Press.
704   Blum, M.D., Roberts, H.H., 2009. Drowning of the Mississippi Delta due to insufficient sediment supply
705   and global sea-level rise. Nature Geoscience 2, 488–491.
706   Boesch, D.F., Turner, R.E., 1984. Dependence of fishery species on salt marshes: The role of food and
707   refuge. Estuaries 7, 460–468. https://doi.org/10.2307/1351627
708   Boorman, L., Hazelden, J., Boorman, M., 2002. New Salt Marshes for Old - Salt Marsh Creation and
709   Management 11.
710   Bopp, R.F., Simpson, H.J., Chillrud, S.N., Robinson, D.W., 1993. Sediment-derived chronologies of
711   persistent contaminants in Jamaica Bay, New York. Estuaries 16, 608–616.
712   Bouma, T.J., Vries, M.B.De., Low, E., Kusters, L., Herman, P.M.J., Tánczos, I.C., Temmerman, S., Hesselink,
713   A., Meire, P., Regenmortel, S. van., 2005. Flow hydrodynamics on a mudflat and in salt marsh
714   vegetation: identifying general relationships for habitat characterisations. Hydrobiologia 540,
715   259–274. https://doi.org/10.1007/s10750-004-7149-0
716   Brain, M.J., Kemp, A.C., Hawkes, A.D., Engelhart, S.E., Vane, C.H., Cahill, N., Hill, T.D., Donnelly, J.P.,
717   Horton, B.P., 2017. Exploring mechanisms of compaction in salt-marsh sediments using Common
718   Era relative sea-level reconstructions. Quaternary Science Reviews 167, 96–111.
719   https://doi.org/10.1016/j.quascirev.2017.04.027
720   Braswell, A.E., Heffernan, J.B., Kirwan, M.L., (2020). How old are marshes on the East Coast, USA?
721   Complex patterns in wetland age within and among regions. Geophysical Research Letters n/a,
722   e2020GL089415. https://doi.org/10.1029/2020GL089415
723   Brin, L.D., Valiela, I., Goehringer, D., Howes, B., 2010. Nitrogen interception and export by experimental
724   salt marsh plots exposed to chronic nutrient addition. Marine Ecology Progress Series 400, 3–17.
725   https://doi.org/10.3354/meps08460
726   Broome, S.W., Craft, C.B., Burchell, M.R., 2019. Chapter 22 - Tidal Marsh Creation, in: Perillo, G.M.E.,
727   Wolanski, E., Cahoon, D.R., Hopkinson, C.S. (Eds.), Coastal Wetlands. Elsevier, pp. 789–816.
728   https://doi.org/10.1016/B978-0-444-63893-9.00022-8
729   Buffington, K.J., Dugger, B.D., Thorne, K.M., Takekawa, J.Y., 2016. Statistical correction of lidar-derived
730   digital elevation models with multispectral airborne imagery in tidal marshes. Remote Sensing of
731   Environment 186, 616–625. https://doi.org/10.1016/j.rse.2016.09.020
732   Cahoon, D.R., Reed, D.J., Day, J.W., 1995. Estimating shallow subsidence in microtidal salt marshes of
733   the southeastern United States: Kaye and Barghoorn revisited. Marine Geology 128, 1–9.
734   https://doi.org/10.1016/0025-3227(95)00087-F
735   Chen, Z., Saito, Y., Kanai, Y., Wei, T., Li, L., Yao, H., Wang, Z., 2004. Low concentration of heavy metals in
736   the Yangtze estuarine sediments, China: a diluting setting. Estuarine, Coastal and Shelf Science
737   60, 91–100.

738 Chou, C., Peteet, D., 2009. Macrofossil evidence for Middle to Late Holocene vegetation shifts at Iona
739   Island Marsh, Hudson Valley, NY. Final Report of the Tibor T. Polgar Fellowship Program.
740 Cochard, R., Ranamukhaarachchi, S.L., Shivakoti, G.P., Shipin, O.V., Edwards, P.J., Seeland, K.T., 2008.
741   The 2004 tsunami in Aceh and Southern Thailand: a review on coastal ecosystems, wave hazards
742   and vulnerability. Perspectives in Plant Ecology, Evolution and Systematics 10, 3–40.
743 Collins, M.J., Miller, D., 2012. Upper Hudson River Estuary (usa) Floodplain Change Over the 20th
744   Century. River Research and Applications 28, 1246–1253. https://doi.org/10.1002/rra.1509
745 Cook, T.L., Yellen, B.C., Woodruff, J.D., Miller, D., 2015. Contrasting human versus climatic impacts on
746   erosion. Geophysical Research Letters 42, 6680–6687. https://doi.org/10.1002/2015GL064436
747 Craft, C., Broome, S., Campbell, C., 2002. Fifteen Years of Vegetation and Soil Development after
748   Brackish-Water Marsh Creation. Restoration Ecology 10, 248–258.
749   https://doi.org/10.1046/j.1526-100X.2002.01020.x
750 Crosby, S.C., Sax, D.F., Palmer, M.E., Booth, H.S., Deegan, L.A., Bertness, M.D., Leslie, H.M., 2016. Salt
751   marsh persistence is threatened by predicted sea-level rise. Estuarine, Coastal and Shelf Science
752   181, 93–99. https://doi.org/10.1016/j.ecss.2016.08.018
753 Croudace, I.W., Rindby, A., Rothwell, R.G., 2006. ITRAX: description and evaluation of a new multi-
754   function X-ray core scanner. Geological Society, London, Special Publications 267, 51–63.
755 Darke, A.K., Megonigal, J.P., 2003. Control of sediment deposition rates in two mid-Atlantic Coast tidal
756   freshwater wetlands. Estuarine, Coastal and Shelf Science 57, 255–268.
757   https://doi.org/10.1016/S0272-7714(02)00353-0
758 Dean, W.E., 1974. Determination of carbonate and organic matter in calcareous sediments and
759   sedimentary rocks by loss on ignition; comparison with other methods. Journal of Sedimentary
760   Research 44, 242–248.
761 Delgado, P., Hensel, P.F., Swarth, C.W., Ceroni, M., Boumans, R., 2013. Sustainability of a Tidal
762   Freshwater Marsh Exposed to a Long-term Hydrologic Barrier and Sea Level Rise: A Short-term
763   and Decadal Analysis of Elevation Change Dynamics. Estuaries and Coasts 36, 585–594.
764   https://doi.org/10.1007/s12237-013-9587-2
765 Emery, K.O., Wigley, R.L., Rubin, M., 1965. A Submerged Peat Deposit Off the Atlantic Coast of the
766   United States1. Limnology and Oceanography 10, R97–R102.
767   https://doi.org/10.4319/lo.1965.10.suppl2.r97
768 Ewers Lewis, C.J., Baldock, J.A., Hawke, B., Gadd, P.S., Zawadzki, A., Heijnis, H., Jacobsen, G.E., Rogers, K.,
769   Macreadie, P.I., 2019. Impacts of land reclamation on tidal marsh 'blue carbon' stocks. Science
770   of The Total Environment 672, 427–437. https://doi.org/10.1016/j.scitotenv.2019.03.345
771 Faber, M., 2002. Soil survey of Dutchess County, New York.
772 FitzGerald, D.M., Hughes, Z., 2019. Marsh Processes and Their Response to Climate Change and Sea-
773   Level Rise. Annual Review of Earth and Planetary Sciences 47, 481–517.
774   https://doi.org/10.1146/annurev-earth-082517-010255
775 Foster, D.R., 1992. Land-Use History (1730-1990) and Vegetation Dynamics in Central New England, USA.
776   Journal of Ecology 80, 753–771. https://doi.org/10.2307/2260864
777 French, J.R., Spencer, T., 1993. Dynamics of sedimentation in a tide-dominated backbarrier salt marsh,
778   Norfolk, UK. Marine Geology 110, 315–331. https://doi.org/10.1016/0025-3227(93)90091-9
779 Gedan, K.B., Kirwan, M.L., Wolanski, E., Barbier, E.B., Silliman, B.R., 2011. The present and future role of
780   coastal wetland vegetation in protecting shorelines: answering recent challenges to the
781   paradigm. Climatic Change 106, 7–29. https://doi.org/10.1007/s10584-010-0003-7
782 Gu, J., Luo, M., Zhang, X., Christakos, G., Agusti, S., Duarte, C.M., Wu, J., 2018. Losses of salt marsh in
783   China: Trends, threats and management. Estuarine, Coastal and Shelf Science 214, 98–109.
784   https://doi.org/10.1016/j.ecss.2018.09.015

785 Hartig, E.K., Gornitz, V., Kolker, A., Mushacke, F., Fallon, D., 2002. Anthropogenic and climate-change
786   impacts on salt marshes of Jamaica Bay, New York City. Wetlands 22, 71–89.
787 Hilfinger IV, M.F., Mullins, H.T., Burnett, A., Kirby, M.E., 2001. A 2500 year sediment record from
788   Fayetteville Green Lake, New York: evidence for anthropogenic impacts and historic isotope
789   shift. Journal of Paleolimnology 26, 293–305. https://doi.org/10.1023/A:1017560300681
790 Hofstede, J.L.A., 2003. Integrated management of artificially created salt marshes in the Wadden Sea of
791   Schleswig-Holstein, Germany. Wetlands Ecology and Management 11, 183–194.
792   https://doi.org/10.1023/A:1024248127037
793 Kemp, A.C., Hill, T.D., Vane, C.H., Cahill, N., Orton, P.M., Talke, S.A., Parnell, A.C., Sanborn, K., Hartig,
794   E.K., 2017. Relative sea-level trends in New York City during the past 1500 years. The Holocene
795   27, 1169–1186.
796 Kirwan, M.L., Murray, A.B., Donnelly, J.P., Corbett, D.R., 2011. Rapid wetland expansion during European
797   settlement and its implication for marsh survival under modern sediment delivery rates.
798   Geology 39, 507–510. https://doi.org/10.1130/G31789.1
799 Kneib, R.T., 1997. The role of tidal marshes in the ecology of estuarine nekton. Oceanography and
800   Marine Biology 35, 163–220.
801 Knutson, P.L., Brochu, R.A., Seelig, W.N., Inskeep, M., 1982. Wave damping inSpartinaalterniflora
802   marshes. Wetlands 2, 87–104. https://doi.org/10.1007/BF03160548
803 Kudish, M., 2000. The Catskill forest: a history. Purple Mountain Press.
804 LaSalle, M.W., Landin, M.C., Sims, J.G., 1991. Evaluation of the flora and fauna of aSpartina alterniflora
805   marsh established on dredged material in Winyah Bay, South Carolina. Wetlands 11, 191–208.
806   https://doi.org/10.1007/BF03160849
807 Lechêne, A., Boët, P., Laffaille, P., Lobry, J., 2018. Nekton communities of tidally restored marshes: A
808   whole-estuary approach. Estuarine, Coastal and Shelf Science 207, 368–382.
809   https://doi.org/10.1016/j.ecss.2017.08.038
810 Long, A.J., Waller, M.P., Stupples, P., 2006. Driving mechanisms of coastal change: Peat compaction and
811   the destruction of late Holocene coastal wetlands. Marine Geology 225, 63–84.
812   https://doi.org/10.1016/j.margeo.2005.09.004
813 Mariotti, G., Elsey-Quirk, T., Bruno, G., Valentine, K., n.d. Mud-associated organic matter and its direct
814   and indirect role in marsh organic matter accumulation and vertical accretion. Limnology and
815   Oceanography n/a. https://doi.org/10.1002/lno.11475
816 McHale, M.R., Siemion, J., 2014. Turbidity and suspended sediment in the upper Esopus Creek
817   watershed, Ulster County, New York. US Geological Survey.
818 Meade, R.H., 1982. Sources, Sinks, and Storage of River Sediment in the Atlantic Drainage of the United
819   States. The Journal of Geology 90, 235–252. https://doi.org/10.1086/628677
820 Meier, D., 2004. Man and environment in the marsh area of Schleswig–Holstein from Roman until late
821   Medieval times. Quaternary International, Geological processes and human interaction on the
822   German North Sea coast 112, 55–69. https://doi.org/10.1016/S1040-6182(03)00065-X
823 Miller, D., Ladd, J., Nieder, W.C., 2006. Channel morphology in the Hudson River Estuary: Historical
824   changes and opportunities for restoration, in: American Fisheries Society Symposium. American
825   Fisheries Society, p. 29.
826 Minello, T.J., Rozas, L.P., Baker, R., 2012. Geographic Variability in Salt Marsh Flooding Patterns may
827   Affect Nursery Value for Fishery Species. Estuaries and Coasts 35, 501–514.
828   https://doi.org/10.1007/s12237-011-9463-x
829 Morris, J.T., Barber, D.C., Callaway, J.C., Chambers, R., Hagen, S.C., Hopkinson, C.S., Johnson, B.J.,
830   Megonigal, P., Neubauer, S.C., Troxler, T., Wigand, C., 2016. Contributions of organic and
831   inorganic matter to sediment volume and accretion in tidal wetlands at steady state. Earth's
832   Future 4, 110–121. https://doi.org/10.1002/2015EF000334

833   Neckles, H.A., Dionne, M., Burdick, D.M., Roman, C.T., Buchsbaum, R., Hutchins, E., 2002. A Monitoring
834   Protocol to Assess Tidal Restoration of Salt Marshes on Local and Regional Scales. Restoration
835   Ecology 10, 556–563. https://doi.org/10.1046/j.1526-100X.2002.02033.x
836   Nelson, J.L., Zavaleta, E.S., 2012. Salt Marsh as a Coastal Filter for the Oceans: Changes in Function with
837   Experimental Increases in Nitrogen Loading and Sea-Level Rise. PLOS ONE 7, e38558.
838   https://doi.org/10.1371/journal.pone.0038558
839   Neubauer, S.C., 2008. Contributions of mineral and organic components to tidal freshwater marsh
840   accretion. Estuarine, Coastal and Shelf Science 78, 78–88.
841   Nitsche, F.O., Ryan, W.B.F., Carbotte, S.M., Bell, R.E., Slagle, A., Bertinado, C., Flood, R., Kenna, T.,
842   McHugh, C., 2007. Regional patterns and local variations of sediment distribution in the Hudson
843   River Estuary. Estuarine, Coastal and Shelf Science, Sedimentological and ecohydrological
844   processes of Asian deltas: The Yangtze and the Mekong 71, 259–277.
845   https://doi.org/10.1016/j.ecss.2006.07.021
846   Nolte, S., Koppenaal, E.C., Esselink, P., Dijkema, K.S., Schuerch, M., De Groot, A.V., Bakker, J.P.,
847   Temmerman, S., 2013. Measuring sedimentation in tidal marshes: a review on methods and
848   their applicability in biogeomorphological studies. J Coast Conserv 17, 301–325.
849   https://doi.org/10.1007/s11852-013-0238-3
850   Odum, W.E., 1988. Comparative ecology of tidal freshwater and salt marshes. Annual Review of Ecology
851   and Systematics 19, 147–176.
852   Olsen, C.R., Simpson, H.J., Bopp, R.F., Williams, S.C., Peng, T.H., Deck, B.L., 1978. A geochemical analysis
853   of the sediments and sedimentation in the Hudson Estuary. Journal of Sedimentary Research 48,
854   401–418. https://doi.org/10.1306/212F7496-2B24-11D7-8648000102C1865D
855   Olsson, K.S., 1981. Soil Survey of Orange County, New York. U.S. Department of Agriculture, Soil
856   Conservation Service.
857   Palinkas, C.M., Engelhardt, K.A.M., 2016. Spatial and temporal patterns of modern (100 yr)
858   sedimentation in a tidal freshwater marsh: Implications for future sustainability. Limnology and
859   Oceanography 61, 132–148. https://doi.org/10.1002/lno.10202
860   Panuzio, F.L., 1965. Lower Hudson River Siltation. Proceedings of the Federal InterAgency Sedimentation
861   Conference. Agricultural Research Service 512–550.
862   Pederson, D.C., Peteet, D.M., Kurdyla, D., Guilderson, T., 2005. Medieval Warming, Little Ice Age, and
863   European impact on the environment during the last millennium in the lower Hudson Valley,
864   New York, USA. Quaternary Research 63, 238–249. https://doi.org/10.1016/j.yqres.2005.01.001
865   Pennington, W., Tutin, T.G., Cambray, R.S., Fisher, E.M., 1973. Observations on lake sediments using
866   fallout 137Cs as a tracer. Nature 242, 324.
867   Peteet, D.M., Nichols, J., Kenna, T., Chang, C., Browne, J., Reza, M., Kovari, S., Liberman, L., Stern-Protz,
868   S., 2018. Sediment starvation destroys New York City marshes' resistance to sea level rise. PNAS
869   115, 10281–10286. https://doi.org/10.1073/pnas.1715392115
870   Ralston, D., Yellen, B., Woodruff, J., 2020. Watershed sediment supply and potential impacts of dam
871   removals for an estuary [WWW Document]. Earth and Space Science Open Archive.
872   https://doi.org/10.1002/essoar.10502519.1
873   Ralston, D.K., Geyer, W.R., Lerczak, J.A., 2008. Subtidal salinity and velocity in the Hudson River estuary:
874   Observations and modeling. Journal of Physical Oceanography 38, 753–770.
875   Ralston, D.K., Talke, S., Geyer, W.R., Al-Zubaidi, H.A., Sommerfield, C.K., 2019. Bigger tides, less flooding:
876   Effects of dredging on barotropic dynamics in a highly modified estuary. Journal of Geophysical
877   Research: Oceans 124, 196–211.
878   Ralston, D.K., Warner, J.C., Geyer, W.R., Wall, G.R., 2013. Sediment transport due to extreme events:
879   The Hudson River estuary after tropical storms Irene and Lee. Geophysical Research Letters 40,
880   5451–5455. https://doi.org/10.1002/2013GL057906

881   Rayburn, J.A., Franzi, D.A., Knuepfer, P.L.K., 2007. Evidence from the Lake Champlain Valley for a later
882   onset of the Champlain Sea and implications for late glacial meltwater routing to the North
883   Atlantic. Palaeogeography, Palaeoclimatology, Palaeoecology, North American late-Quaternary
884   meltwater and floods to the ocean: evidence and impact 246, 62–74.
885   https://doi.org/10.1016/j.palaeo.2006.10.027
886   Redfield, A.C., 1972. Development of a New England salt marsh. Ecological monographs 42, 201–237.
887   Schuerch, M., Spencer, T., Temmerman, S., Kirwan, M.L., Wolff, C., Lincke, D., McOwen, C.J., Pickering,
888   M.D., Reef, R., Vafeidis, A.T., Hinkel, J., Nicholls, R.J., Brown, S., 2018. Future response of global
889   coastal wetlands to sea-level rise. Nature 561, 231–234. https://doi.org/10.1038/s41586-018-
890   0476-5
891   Sholkovitz, E.R., 1976. Flocculation of dissolved organic and inorganic matter during the mixing of river
892   water and seawater. Geochimica et Cosmochimica Acta 40, 831–845.
893   https://doi.org/10.1016/0016-7037(76)90035-1
894   Smith, R.H., 1955. Experimental control of water chestnut (Trapa natans) in New York State. New York
895   Fish and Game Journal 2, 173–193.
896   Spencer, T., Schuerch, M., Nicholls, R.J., Hinkel, J., Lincke, D., Vafeidis, A.T., Reef, R., McFadden, L.,
897   Brown, S., 2016. Global coastal wetland change under sea-level rise and related stresses: The
898   DIVA Wetland Change Model. Global and Planetary Change 139, 15–30.
899   Squires, D.F., 1992. Quantifying anthropogenic shoreline modification of the Hudson River and Estuary
900   from European contact to modern time. Coastal Management 20, 343–354.
901   https://doi.org/10.1080/08920759209362183
902   Sritrairat, S., Peteet, D.M., Kenna, T.C., Sambrotto, R., Kurdyla, D., Guilderson, T., 2012. A history of
903   vegetation, sediment and nutrient dynamics at Tivoli North Bay, Hudson Estuary, New York.
904   Estuarine, Coastal and Shelf Science 102–103, 24–35.
905   https://doi.org/10.1016/j.ecss.2012.03.003
906   Staszak, L.A., Armitage, A.R., 2012. Evaluating Salt Marsh Restoration Success with an Index of
907   Ecosystem Integrity. Journal of Coastal Research 410–418. https://doi.org/10.2112/JCOASTRES-
908   D-12-00075.1
909   Tabak, N.M., Laba, M., Spector, S., 2016. Simulating the Effects of Sea Level Rise on the Resilience and
910   Migration of Tidal Wetlands along the Hudson River. PLoS One 11.
911   https://doi.org/10.1371/journal.pone.0152437
912   Temmerman, S., Govers, G., Wartel, S., Meire, P., 2003. Spatial and temporal factors controlling short-
913   term sedimentation in a salt and freshwater tidal marsh, Scheldt estuary, Belgium, SW
914   Netherlands. Earth Surface Processes and Landforms 28, 739–755.
915   https://doi.org/10.1002/esp.495
916   Thorne, K., MacDonald, G., Guntenspergen, G., Ambrose, R., Buffington, K., Dugger, B., Freeman, C.,
917   Janousek, C., Brown, L., Rosencranz, J., 2018. US Pacific coastal wetland resilience and
918   vulnerability to sea-level rise. Science Advances 4, eaao3270.
919   Törnqvist, T.E., Jankowski, K.L., Li, Y.-X., González, J.L., 2020. Tipping points of Mississippi Delta marshes
920   due to accelerated sea-level rise. Science Advances 6, eaaz5512.
921   https://doi.org/10.1126/sciadv.aaz5512
922   Turner, R.E., Swenson, E.M., Milan, C.S., 2000. Organic and Inorganic Contributions to Vertical Accretion
923   in Salt Marsh Sediments, in: Weinstein, M.P., Kreeger, D.A. (Eds.), Concepts and Controversies in
924   Tidal Marsh Ecology. Springer Netherlands, Dordrecht, pp. 583–595. https://doi.org/10.1007/0-
925   306-47534-0_27
926   Warren, R.S., Fell, P.E., Rozsa, R., Brawley, A.H., Orsted, A.C., Olson, E.T., Swamy, V., Niering, W.A., 2002.
927   Salt marsh restoration in Connecticut: 20 years of science and management. Restoration Ecology
928   10, 497–513.

929 Wolters, M., Garbutt, A., Bakker, J.P., 2005. Salt-marsh restoration: evaluating the success of de-
930   embankments in north-west Europe. Biological Conservation 123, 249–268.
931   https://doi.org/10.1016/j.biocon.2004.11.013
932 Wolters, S., Zeiler, M., Bungenstock, F., 2010. Early Holocene environmental history of sunken
933   landscapes: pollen, plant macrofossil and geochemical analyses from the Borkum Riffgrund,
934   southern North Sea. International Journal of Earth Sciences 99, 1707–1719.
935 Worzel, J.L., Drake, C.L., 1959. Structure Section Across the Hudson River at Nyack, N. Y., from Seismic
936   Observations*. Annals of the New York Academy of Sciences 80, 1092–1105.
937   https://doi.org/10.1111/j.1749-6632.1959.tb49282.x
938 Yan, R., Gao, J., Huang, J., 2019. Modelling the hydrological processes of a Chinese lowland polder and
939   identifying the key factors using an improved PHPS model. Journal of Hydrology 578, 124083.
940   https://doi.org/10.1016/j.jhydrol.2019.124083
941 Yellen, B., Steinschneider, S., 2019. GRADUAL RECOVERY FROM FLOOD DISTURBANCE RECORDED IN
942   SEDIMENT CORES, in: Northeastern Section-54th Annual Meeting-2019. GSA.
943 Yozzo, D.J., Andersen, J.L., Cianciola, M.M., Nieder, W.C., Miller, D.E., Ciparis, S., McAvoy, J., 2005.
944   Ecological Profile of the Hudson River National Estuarine Research Reserve 165.
945 Yozzo, D.J., Wilber, P., Will, R.J., 2004. Beneficial use of dredged material for habitat creation,
946   enhancement, and restoration in New York–New Jersey Harbor. Journal of Environmental
947   Management 73, 39–52. https://doi.org/10.1016/j.jenvman.2004.05.008
948
949

950   TABLES

951 **Table 1**: site characteristics for six wetland study sites within the Hudson River Estuary. Reported
952 catchment areas refer to the tributary catchment that enters the estuary at or near each marsh (see Fig.
953 1). Distance from the Battery, the southern tip of Manhattan Island in New York City is reported in km.
954 Dominant vegetative cover types within these wetlands include cattails (*Typha angustifolia*), *Phragmites*
955 *australis*, invasive water chestnut (*Trapa Natans*), and spatterdock (*Nuphar advena*).

	Stockport	Esopus	Tiv. North	Tiv. South	Vanderburgh	Iona
Site locus area (km2)	0.25	0.11	1.45	1.05	0.36	0.49
Number of cores	3	5	5	3	6	5
Catchment (km2)	1340	1100	55	68	71	7.5
Dist. from Battery (km)	193	163	159.5	157	140	72
Dominant cover	*Typha*	*Phrag/Typha*	*Typha*	Mudflat/ *Trapa*	*Typha/Nuphar /Trapa*	*Phrag/Typha*
Avg Accumulation Rate (cm/yr)	1.0	0.9	0.9	0.6	1.2	0.3

956

957

23

FIGURES
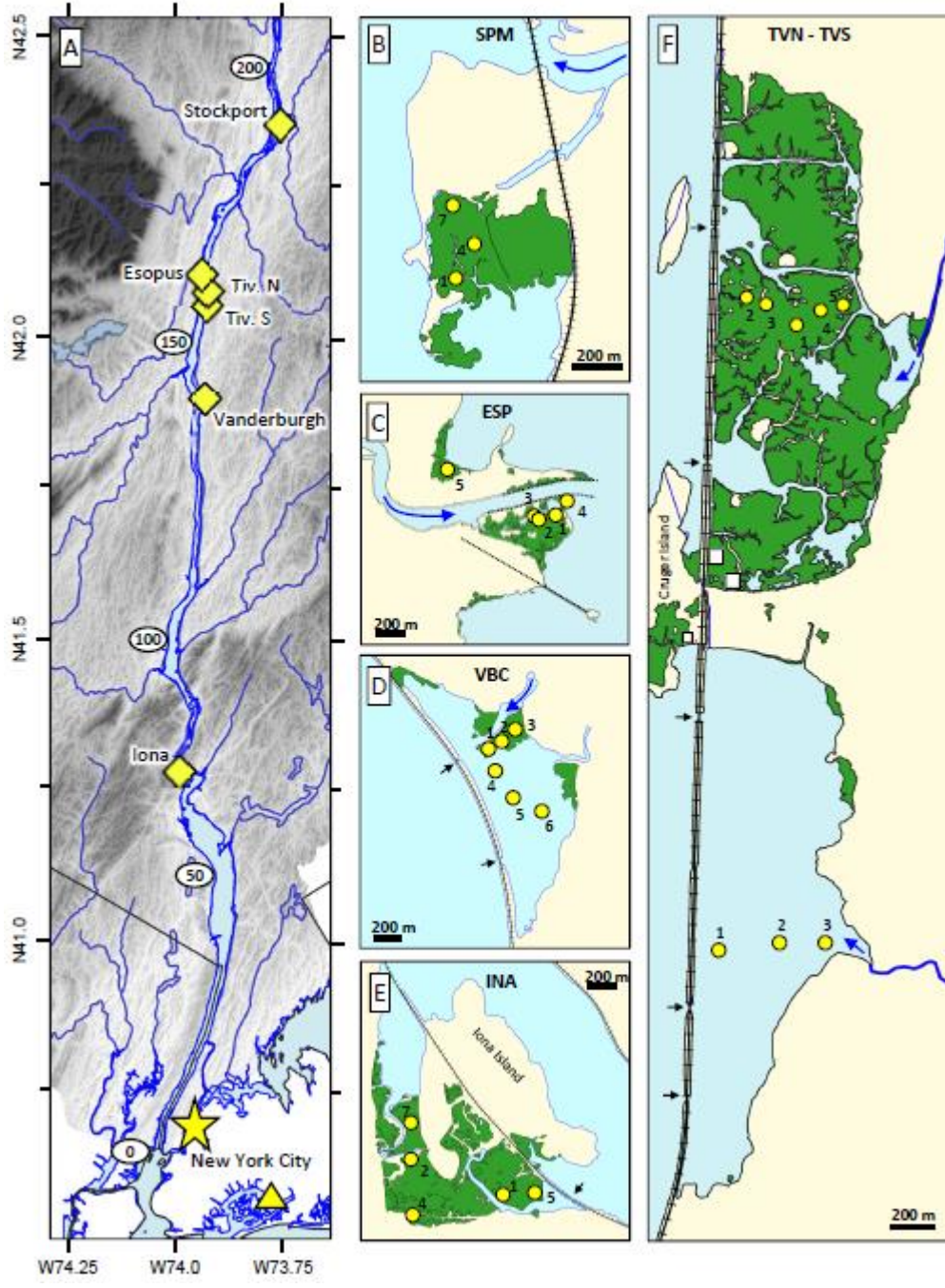
959   S

Fig. 1: Panel A depicts the six study sites (yellow diamonds) along the tidal Hudson River with New York City and
Jamaica Bay (yellow triangle) at the mouth of the river. White ovals denote the distance from the Battery in
kilometers. Panels B, C, D, E, F depict the location of emergent marsh in green at Stockport (SPM), Esopus delta
(ESP), Vanderburg Cove (VBC), Iona Island Marsh (INA), and Tivoli North (TVN) and South (TVS) Bays. White squares
in panel F denote the locations of cores from Sritrairat et al. (2012). Yellow circles indicate the locations and core
number of cores described in the text or in supplementary figures. Hardened structures (jetties and railroad
berms) are shown in black, with black arrows indicating culvert locations. Significant tributary mouths are indicated
with blue arrows.

968
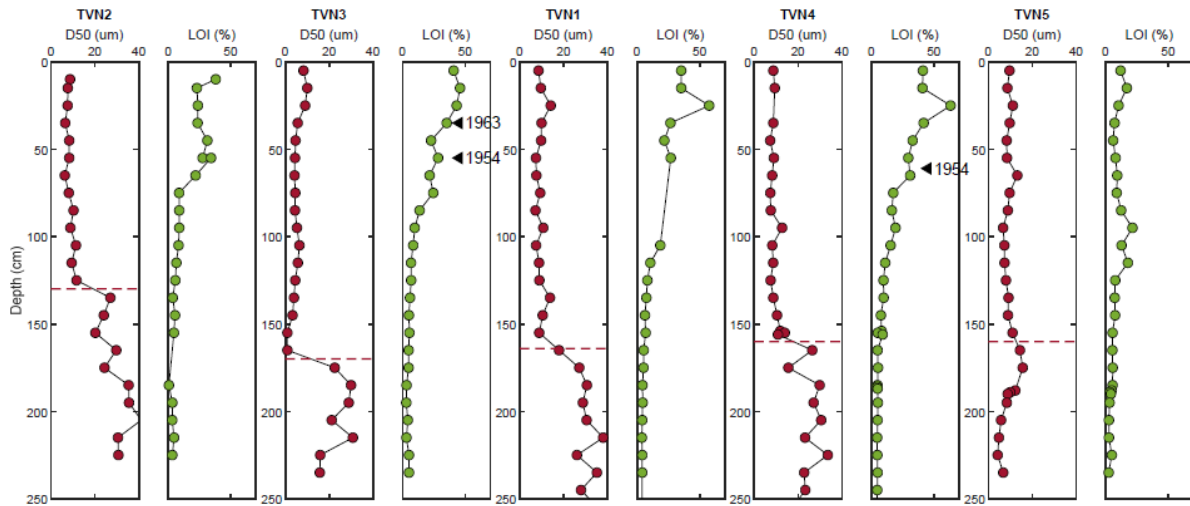
Fig. 2: Tivoli North core transect showing median grain size (red) and LOI (green) for cores from west to east. See Fig. 1 for locations. Dashed lines indicates a sudden drop in grain size in each core. Triangles denote depths of ^{137}Cs derived ages (TVN3 ^{137}Cs data shown in Fig. 3).

974
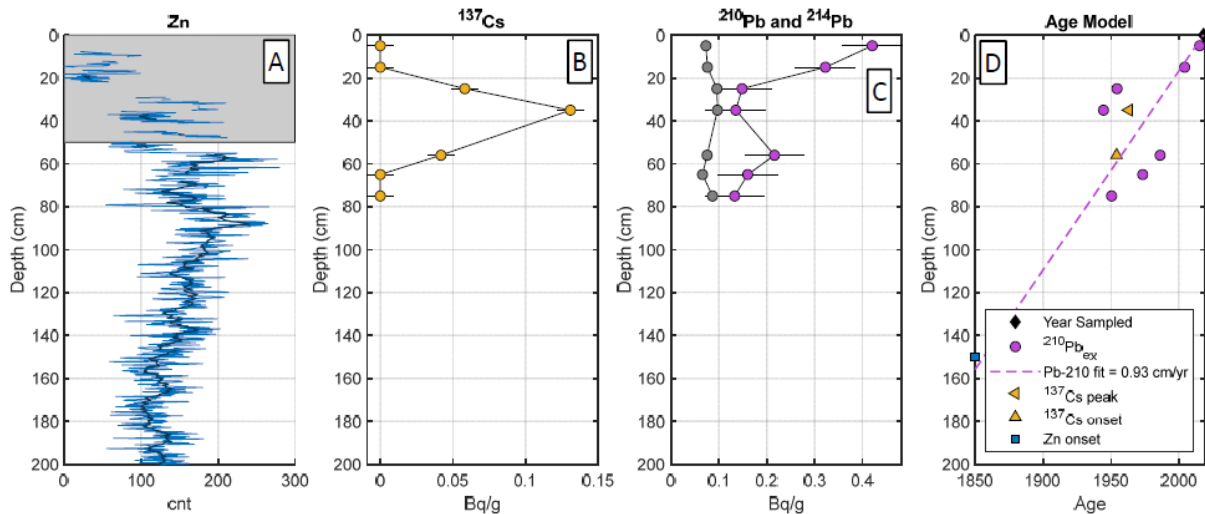
Fig. 3: Depth profiles from TVN3 Core including (A) zinc XRF counts, (B) ^{137}Cs and (C) ^{210}Pb and [214]Pb activities. Error bars in B and C represent instrument measurement uncertainty. Lighter and darker blue lines in A represent raw and 10 pt low pass filter of data and grey box denotes region of poor sampling due to root matter and highly porous surficial sediments. (D) Depth-to-age model based on 1954 onset and 1963 peak in [137]Cs (triangles), unsupported Pb-210 (magenta circles) and an assumed ~1850 CE onset of elevated Zn. Dashed line is 0.9 cm/yr best fit to Pb-210 derived ages age.

25

984
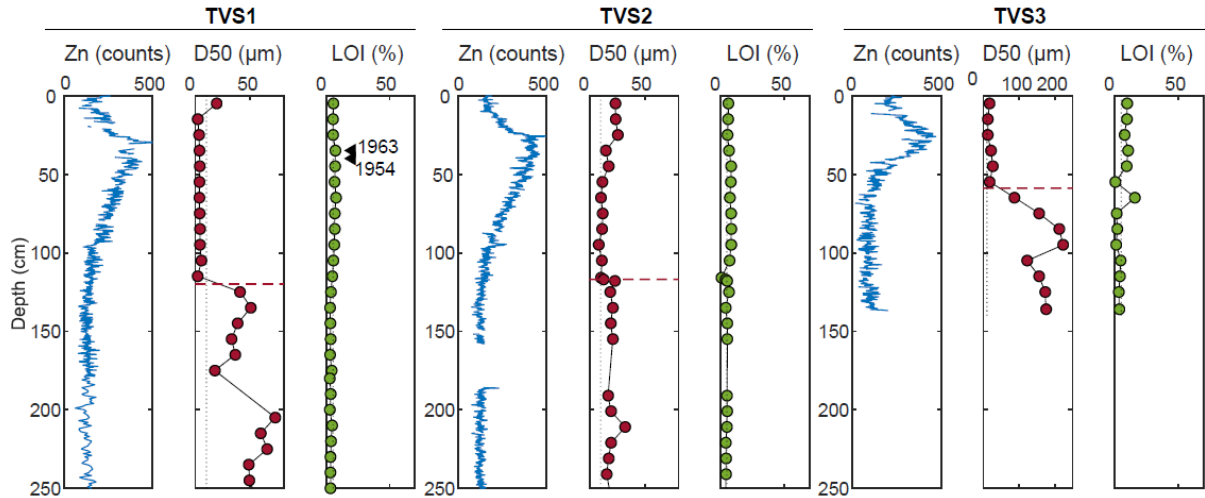
Fig. 4: Depth profiles of Zn (blue), median grain size (D50, red) and LOI (green) for the three core transect from Tivoli Bay South (see Fig. 1 for locations). Note axis for D50 in TVS3 is extended in order to include larger grain sizes observed at this location. A dotted vertical line at 5 µm is provided for reference. Triangles denote depths of ^{137}Cs derived ages for TVS1.

989
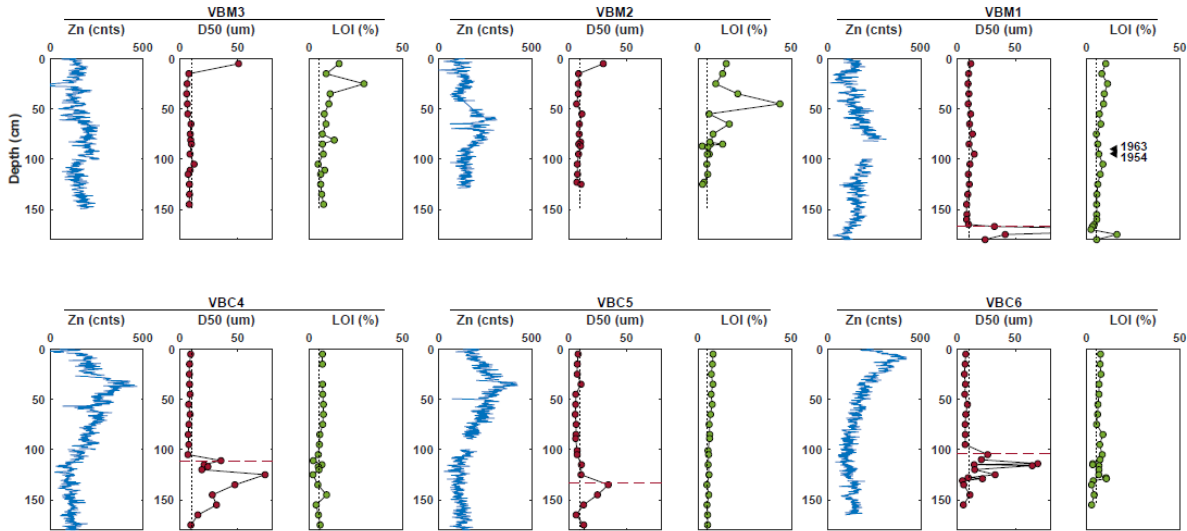
Fig. 5: Vanderburgh Cove depth profiles of Zn (blue), median grain size (D50, red) and LOI (green) for cores from the marsh (top panels) and open water/tidal flat (bottom panels), (see Fig. 1 for locations). Triangles in upper right LOI panel denote depths of ^{137}Cs derived ages for VBM1.

993

994

995

996

997

998

26

999
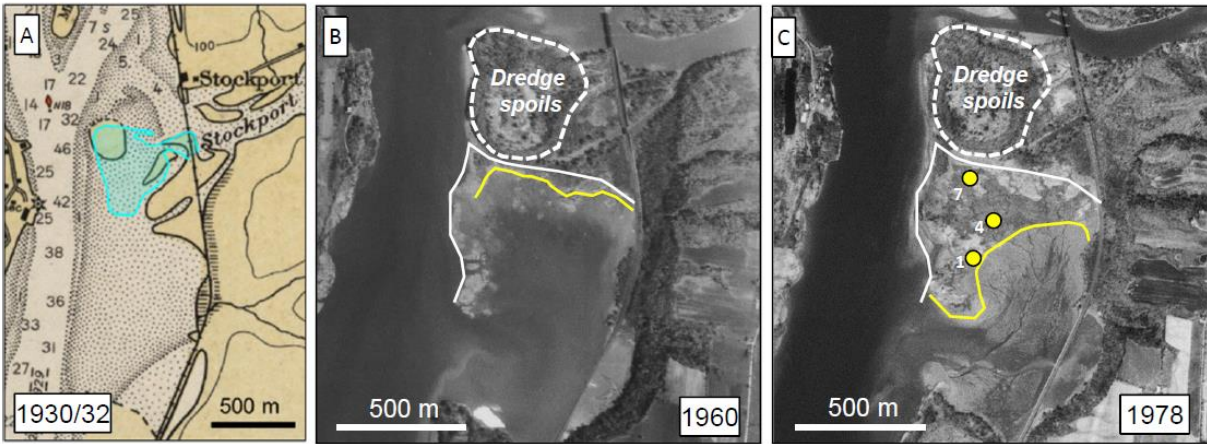
Fig. 6: A historical chart (A) and aerial photos (B, C) depict the development of Stockport Marsh during the mid-20th century. Panel A shows a portion of a 1930 nautical chart (US Coast and Geodetic Survey, 1930) with depths in feet (1 ft = 0.3 m). The shaded blue area depicts the outline of the island at the mouth of Stockport Creek in the 1932 chart revision (US Coast and Geodetic Survey, 1932). Panel B shows the development of a spit southward from the dredge spoils by 1960, with a white line indicating the edge of the interpreted shoreline. The yellow line indicates an interpreted marsh edge. Panel C shows horizontal migration of the marsh over the former shoal area depicted in panel A, with core locations indicated for cores SPM1, SPM4, and SPM7.
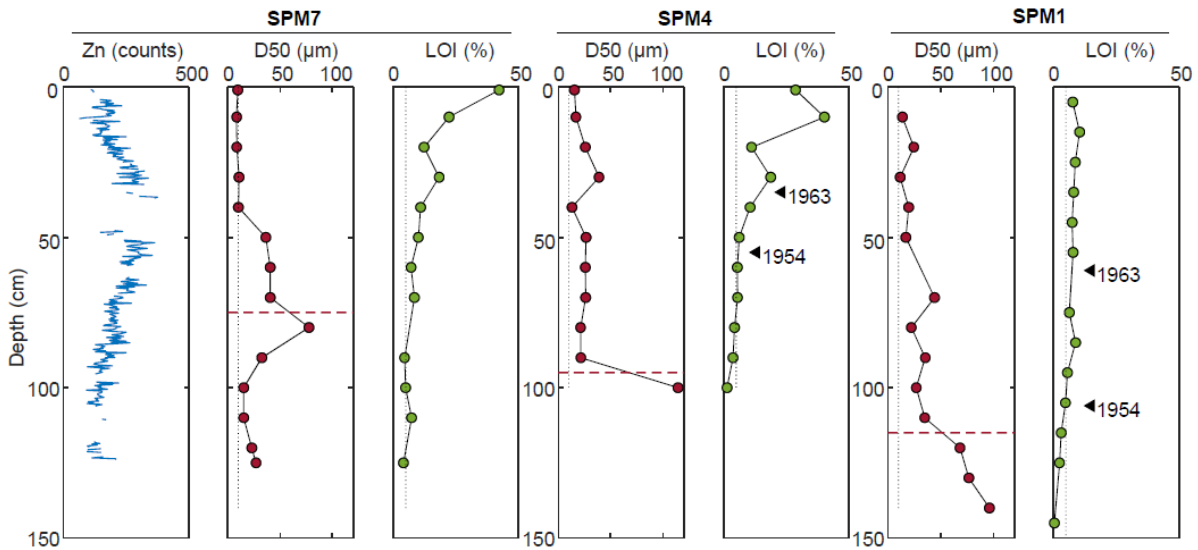
1007

Fig. 7: Stockport Marsh depth profiles of Zn (blue), median grain size (D50, red) and LOI (green). Triangles in LOI panel denote depths of ^{137}Cs derived ages for SPM4 and SPM1. Dashed red line in grain size plots denotes sand-to-mud transition. Zn profiles not shown for SPM4 and SPM1 due to poor data quality.

27

1016

Fig. 8: Esopus Creek's delta at Saugerties, NY in 1863, 1932 and present as depicted in US Coast Survey nautical charts (US Coast Survey, 1863; US Coast and Geodetic Survey, 1932) and current aerial imagery (Google Earth, 2016). Note the appearance of fringing marsh in the 1932 map, followed by its more extensive development towards the modern.

1017
1018
1019
1020

1021
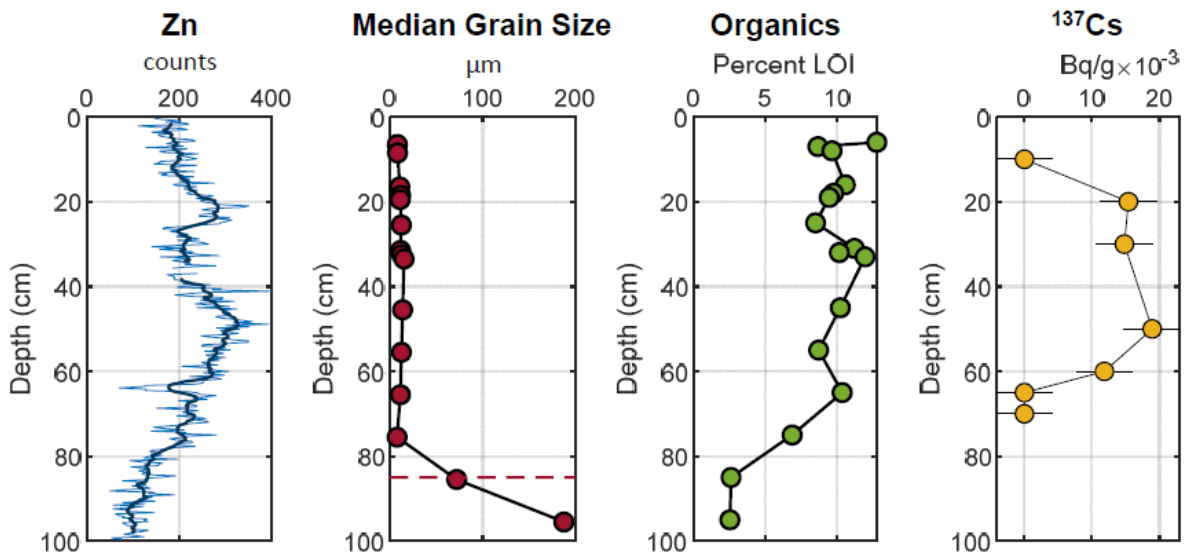
1022

Fig. 9: ESP3 depth profiles of Zn (blue), median grain size (D50, red), LOI (green) and [137]Cs (error bars represent instrument measurement uncertainty).

1023
1024

1025
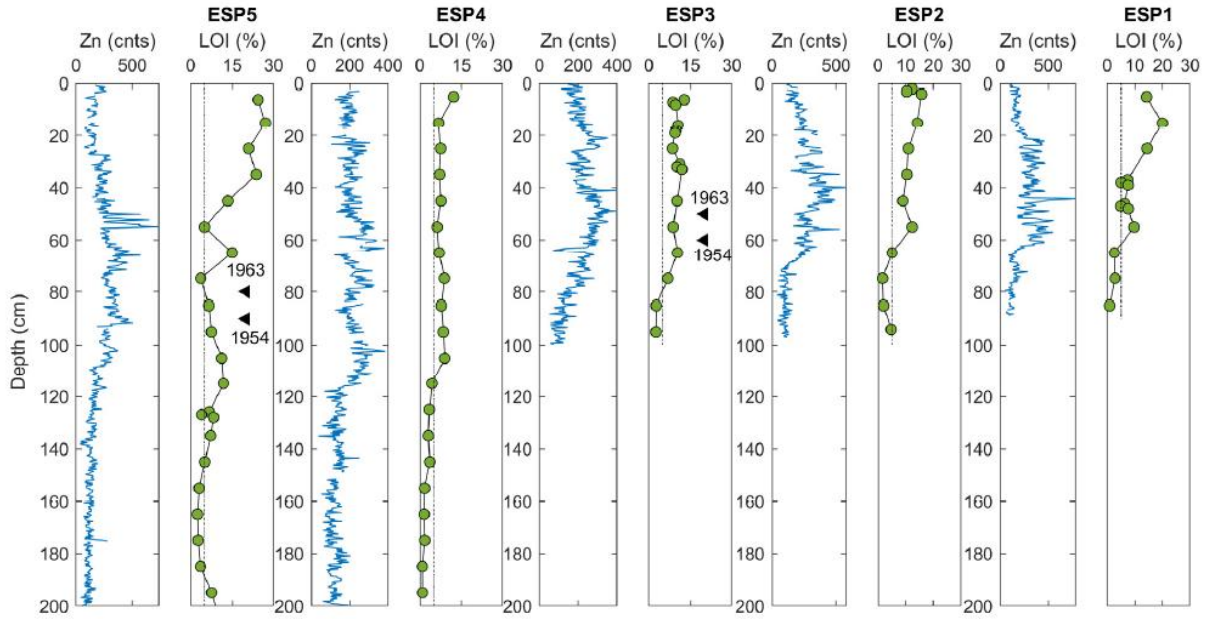
1026

Fig. 10: Depth profiles from tidal wetlands on the Esopus delta of Zn (blue), and LOI (green). Triangles in LOI panel for ESP5 and ESP3 denote depths of ^{137}Cs derived ages (^{137}Cs data for ESP3 shown in Fig. 9).

1029
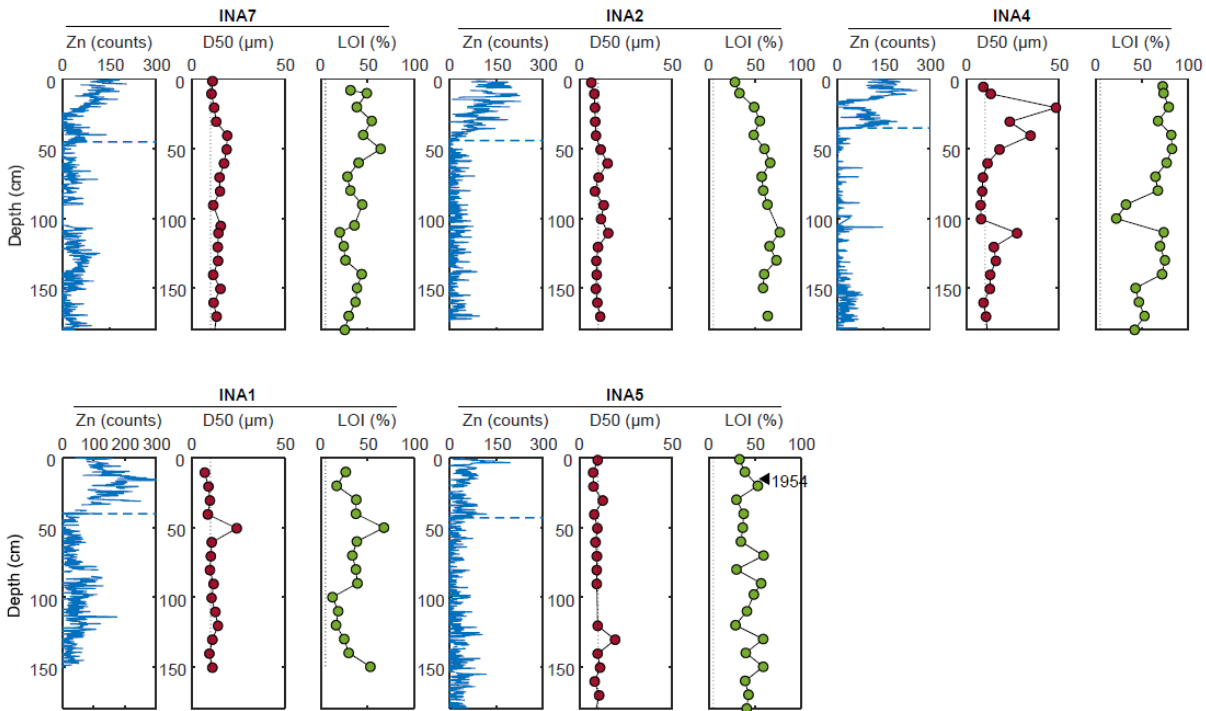
1030

Fig. 11: Depth profiles of Zn (blue), median grain size (D50, red) and LOI (green) for the five core transect from Iona Marsh (see Fig. 1 for locations). A blue line denotes interpreted onset for Zn. Triangles denote depths of ^{137}Cs derived age for INA5.

1034
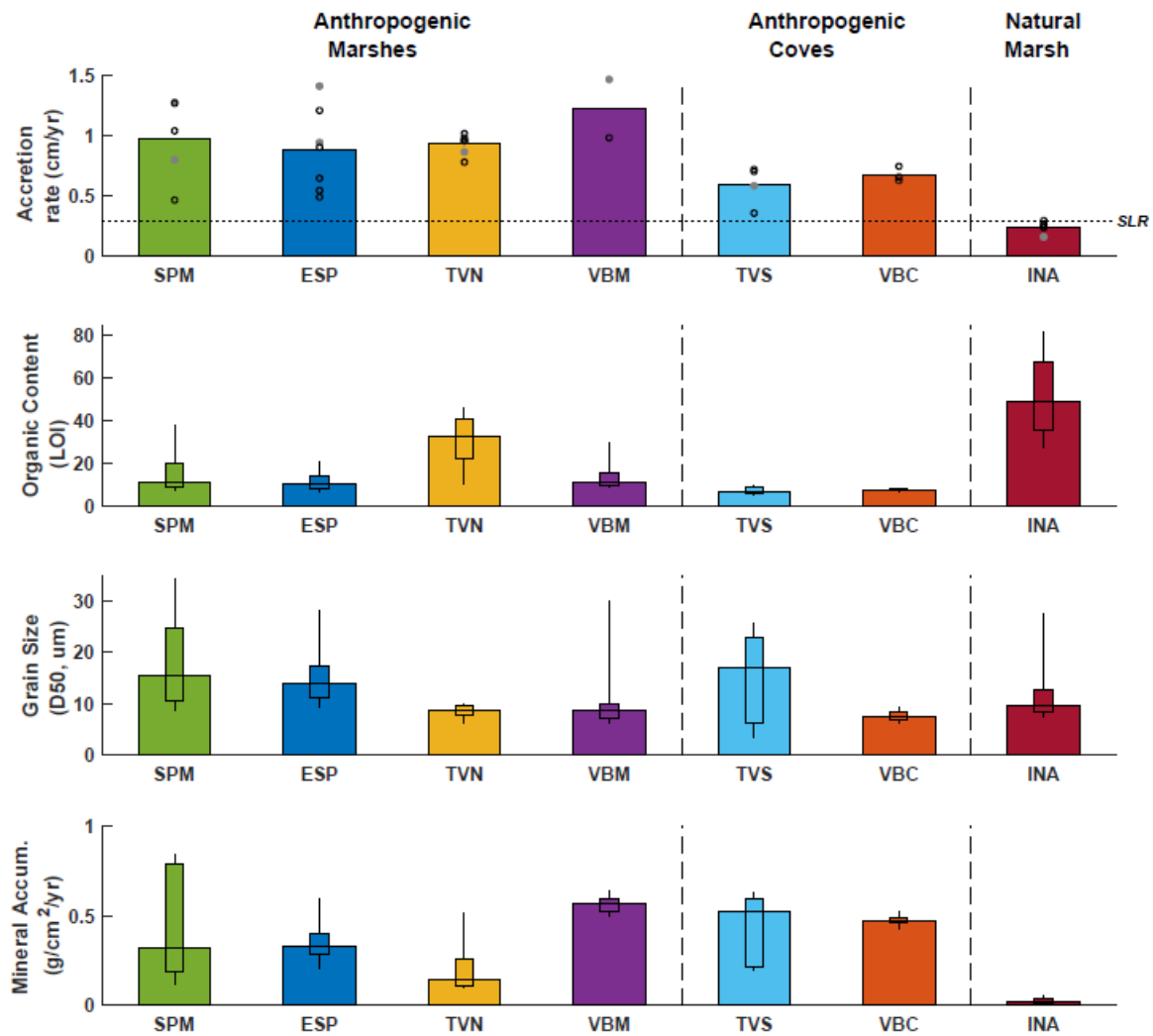
1035

Fig. 12: Distributions of accumulation rates, organic content, median grain size, and inorganic mineral accumulation rates for each study site. Filled gray and open black circles in upper panel are based on 1954 ^{137}Cs onset and Zn chronologies, respectfully. Average rates of relative 20th century sea level rise (SLR) as measured at the Battery, NY (NOAA, 2019), provided as a horizontal dotted line. The wider bar in all plots indicate median value for each site. Inner rectangle in lower three panels represents the 25th and 75th percentiles and ends of outer line the 10th and 90th percentiles of all measurements within top 50 cm.

1043
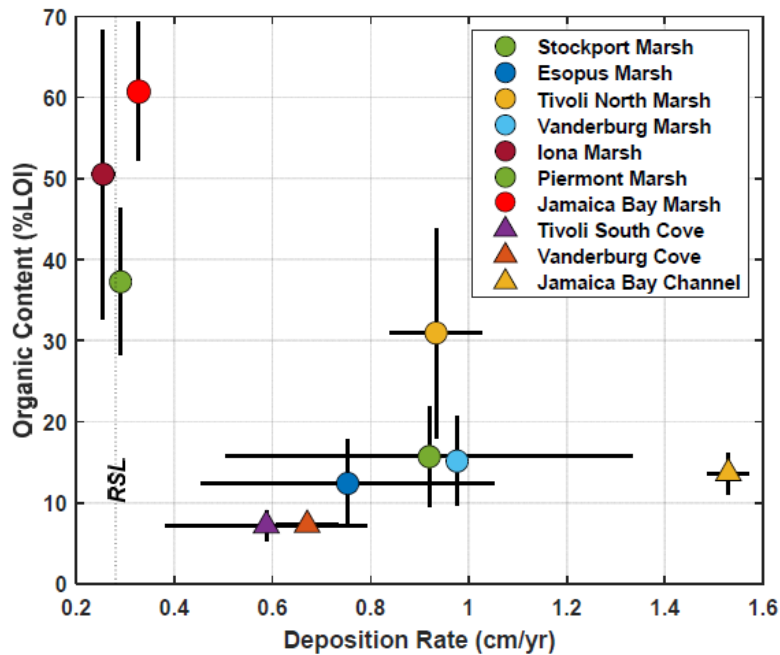
Fig. 13: Average organic content within the top 50 cm of tidal marshes (circles) and muddy environments (triangles) as a function observed deposition rates. Sites from this study include Stockport Marsh (SPM), Esopus Marsh (ESP), Tivoli North Marsh (TVN), Vanderburgh Marsh (VBM), Tivoli South Bay (TVS), Vanderburgh Cove (VBC), and Iona Marsh (INA). Also presented are data from Piermont Marsh (Pederson et al., 2005), Jamaica Bay dredged channel (Bopp et al., 1993), and Jamaica Bay Marsh (Peteet et al., 2018). Error bars represent 1 standard deviation.
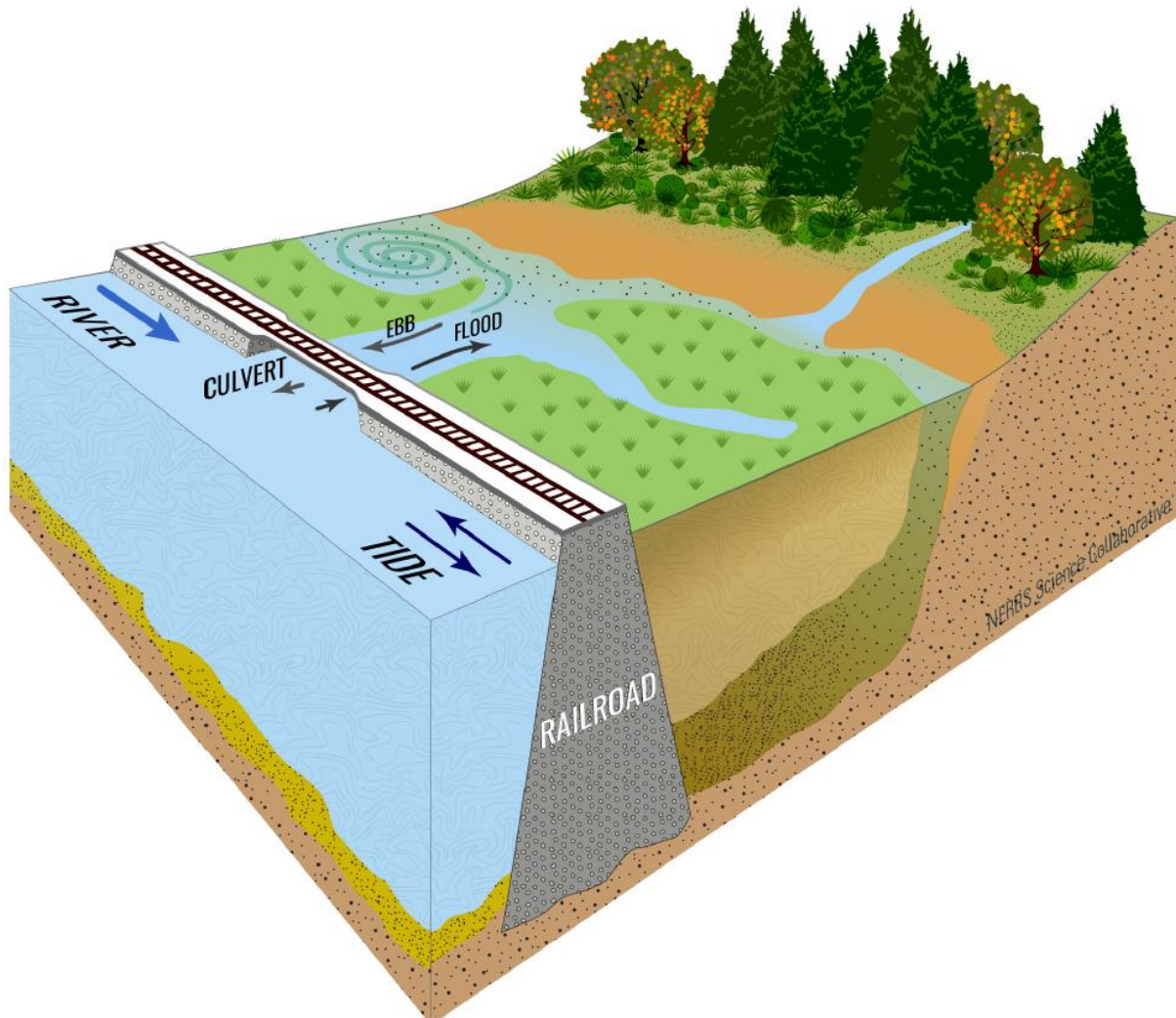
1052

1053   **Fig. 14:** Schematic diagram of mature marsh developed in the shelter of a railroad berm. Thick blue
1054   arrow depicts net river flow, with tidal fluxes indicated in black.

1055

1056

1057
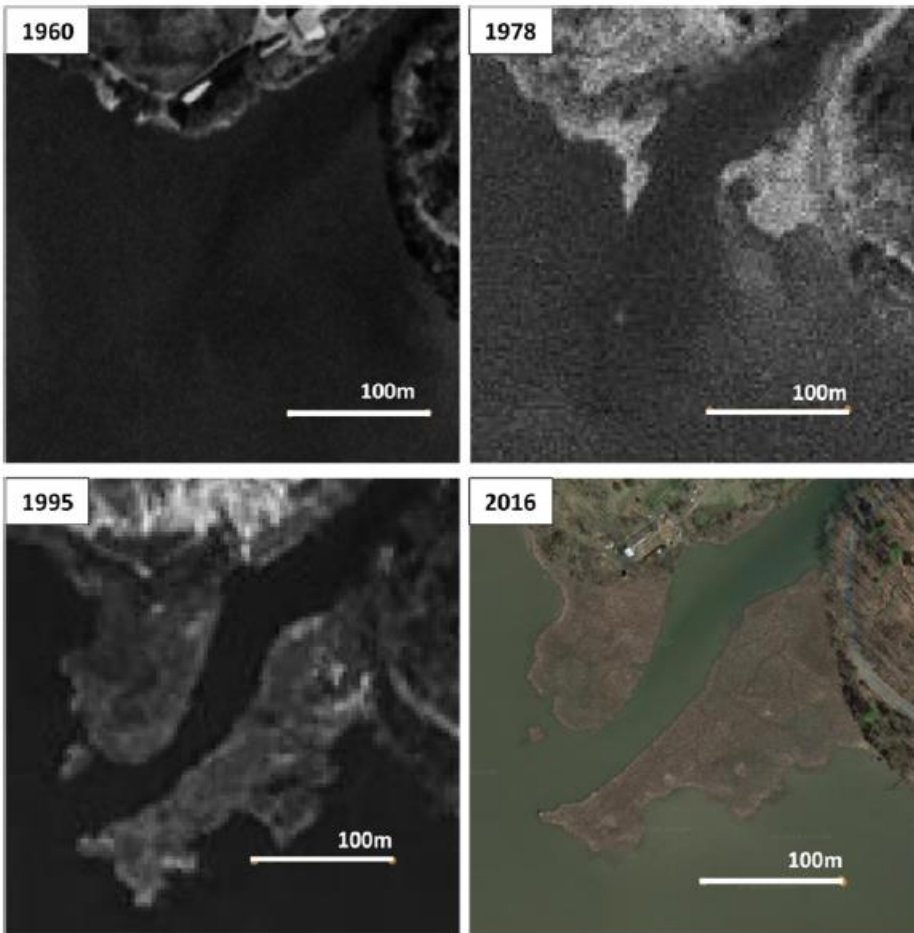
1058

1059 **Supp. Fig. 1 –** Historic air photos of the mouth of Landsman Kill Creek in Vanderburgh Cove (41.88, -
1060 73.93, see Fig 1D for context). No marsh was present in 1960 (top left). Limited marsh had developed by
1061 1978 and expanded rapidly between 1978 and 1995. There does not appear to have been much marsh
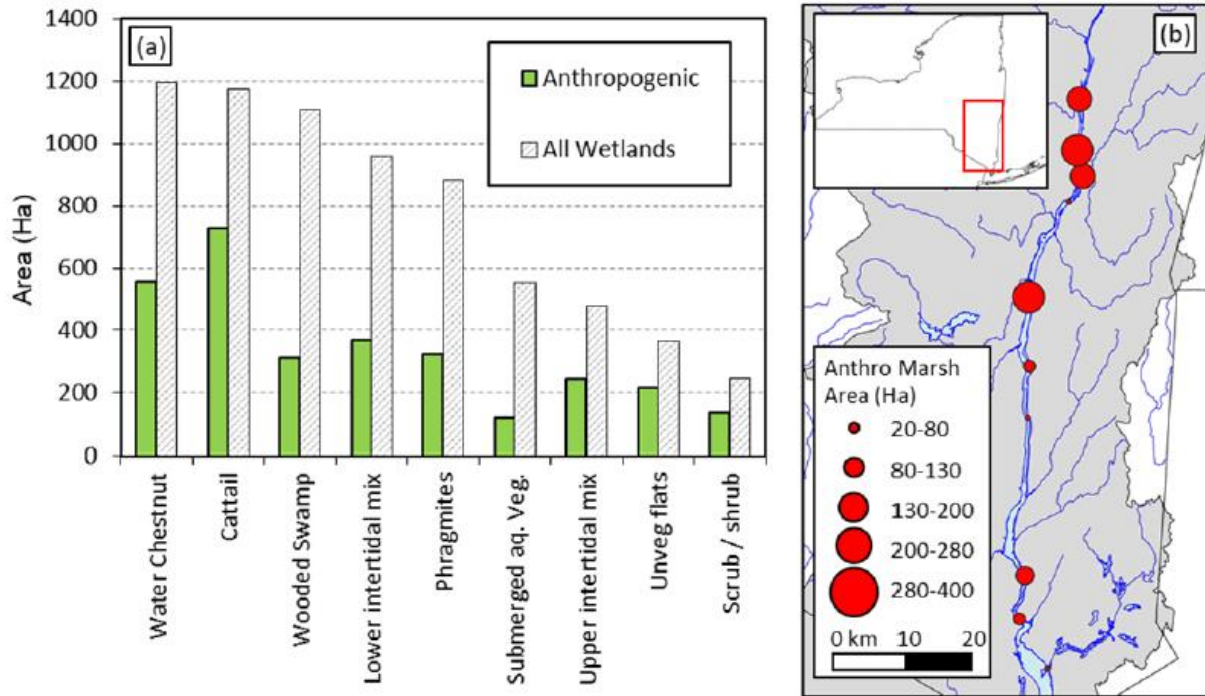1062 expansion between 1995 and 2016. Aerial photos downloaded from earthexplorer.usgs.gov.

1063
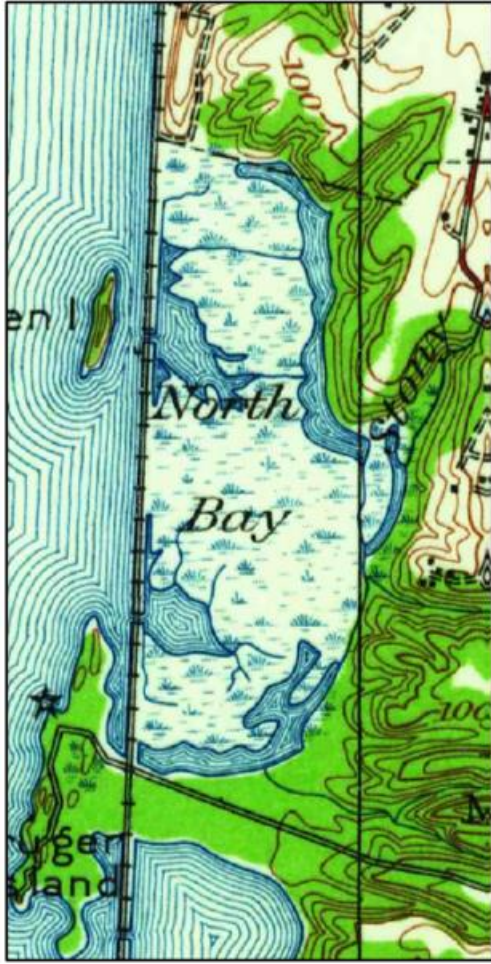
1064

1065 **Supp. Fig. 2** – Tivoli North Bay as depicted in a 1934 USGS topographic map (left) and the same location
1066 in October, 2008 (Google Earth). See Fig. 1 for context within broader Hudson River.

1067

1068

1069   **Supp. Fig. 3 –** (a) Total area of each type of tidal wetland habitat included in the analysis (Geospatial
1070   Data from Cornell, 2011). (b) Geographic distribution of anthropogenic emergent tidal wetlands along
1071   the Hudson River with the watershed shaded grey.

1072
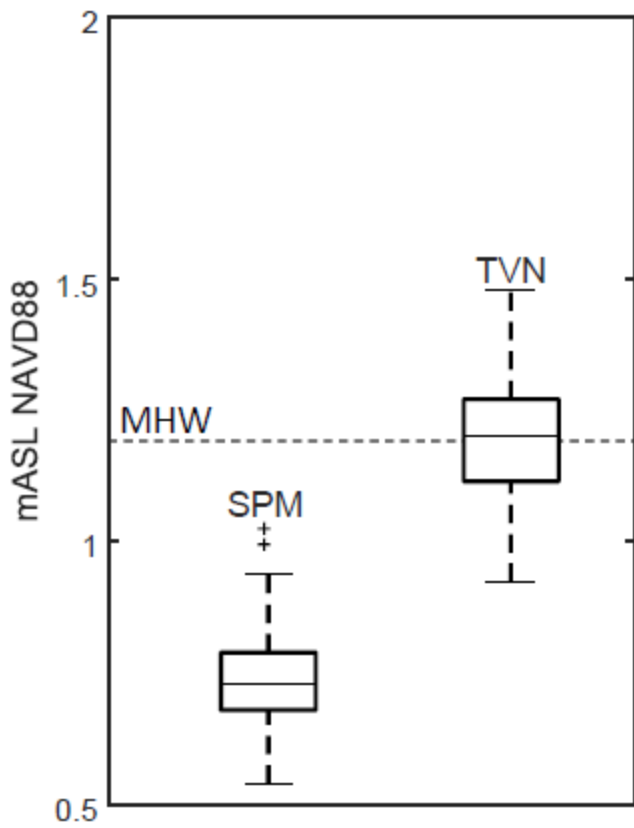
1073
Supp Fig 4 – Box plots of lidar-derived marsh elevations from the marsh platform at Stockport Marsh (SPM) and
Tivoli North Marsh (TVN). Data from NYSDEC (2012). Mean high water (MHW) at Turkey Point tide gauge (NOAA
8518962) located across the river from Tivoli, NY.